

Inter-American University of Puerto Rico
Advance Research and Innovative Experience for students
(ARIES)

EQUIS
Science Report

Inter-American University of Puerto Rico
Advance Research and Innovative Experience for students
(ARIES)

Table of Contents

Bibliography	4
EQUIS Team 2011.....	5
Introduction.....	6
EQUIS Mission Goal	6
Science Objectives	6
Technical Objectives.....	6
HASP EQUIS Requirements	7
Data Preparation - Accelerometer.....	7
Data Preparation – Gyroscope	9
Calibration and Conversion Equations	11
Flight Analysis	12
Phase 1	13
Phase 1 Accelerometer.....	14
Phase 1 Gyroscope.....	14
Phase 1 Magnetometer	15
Phase 1: Internal Temperature	18
Phase II	19
Phase II Accelerometer	19
Phase II Gyroscope	20
Phase II Magnetometer	20
Attitude Determination (Kinematic Equations)	23
Conclusion	30
Appendix A: Calibration Procedure.....	31

Inter-American University of Puerto Rico
Advance Research and Innovative Experience for students
(ARIES)

List of Figures

Figure 1: Accelerometer Raw and Calibrated Data X axis	7
Figure 2: Accelerometer Raw and Calibrated Data Y axis	8
Figure 3: Accelerometer Raw and Calibrated Data Z axis	8
Figure 4: Data Process for Calibration.....	9
Figure 5: Gyroscope Raw and Calibrated Data X axis	9
Figure 6: Gyroscope Raw and Calibrated Data Y axis	10
Figure 7: Gyroscope Raw and Calibrated Data Z axis.....	10
Figure 8: Data Process for Calibration.....	11
Figure 9: Complete flight path HASP 2010 (Sept 31, 2011)	12
Figure 10: Flight Dynamics division by phases	13
Figure 11: Phase one flight path of approx. 2.72 hours	13
Figure 12: Payload Acceleration in three axis during phase 1	14
Figure 13: Phase 1 Gyroscope Data.....	15
Figure 14: Magnetic Magnitude in X, Y and Z axis	16
Figure 15: Field Intensity vs Time during Phase 1	17
Figure 16: 2010 Magnetic Field Intensity [2]	18
Figure 17: Temperature Profile during phase I.....	18
Figure 18: EQUIS 2011 Complete Flight Trajectory.....	19
Figure 19: Phase II Acceleration vs Time.....	19
Figure 20: Phase II Rotational Rate vs time	20
Figure 21: Magnetic Magnitude in X, Y and Z axis	21
Figure 22: Field Intensity vs Time	22
Figure 24: q1 and q2 of the quaternion components of HASP 2010	24
Figure 25: q2 and q3 of the quaternion components of HASP 2010	24
Figure 26: Euler angles for data of HASP 2010	26
Figure 27: Kalman Filter process for converging on a true state vector	27
Figure 28: q1 and q2 of the filtered quaternion components of HASP 2010.....	28
Figure 30: Euler Angles in for x, y and z axes of HASP 2010	29

Inter-American University of Puerto Rico
Advance Research and Innovative Experience for students
(ARIES)

Bibliography

- [1] Granger, D. (n.d.). *LSU Science Space Group*. Retrieved December 5, 2011, from Laspace LSU: <http://laspace.lsu.edu/hasp/Flightinfo-2011.php>
- [2] geomag.models@noaa.gov. (2010, March 6). *NOAA national Geophysical Data Center*. Retrieved December 5, 2011, from The World magnetic model: <http://ngdc.noaa.gov/geomag/WMM/DoDWMM.shtml>
- [3] Wertz, J. R. (1980). *Spacecraft Attitude Determination and Control*. D. Reidel.
- [4] Wertz, J. R. (1999). *Space Mission Analysis and Design*. Space Technology Library.
- [5] Garmin Corporation. (n.d.). Retrieved November 16, 2010, from Garmin Website: HYPERLINK "<http://www8.garmin.com/aboutGPS/>" 1
- [6] Harris, M. B. (2006, September 25). Retrieved November 16, 2010, from HowStuffWorks.com: HYPERLINK "<http://electronics.howstuffworks.com/gadgets/travel/gps.htm>"
<http://electronics.howstuffworks.com/gadgets/travel/gps.htm>
- [7] Trimble. (n.d.). Retrieved November 16, 2010, from Trimble: HYPERLINK "<http://www.trimble.com/gps/index.shtml>" <http://www.trimble.com/gps/index.shtml>
- [8] Corp., S. E. (n.d.). *MicroMag 3-Axis Magnetometer*. Retrieved February 11, 2011, from Sparkfun Electronics: <http://www.sparkfun.com/products/244>
- [9] InvenSense. (2010, 03 30). ITG-3200 Product Specification Revision 1.4. Sunnyvale, CA, US.
- [10] Corp., S. E. (n.d.). *One Wire Digital Temperature Sensor DS18B20*. Retrieved February 10, 2011, from Sparkfun Electronics: HYPERLINK "<http://www.sparkfun.com/products/245>" <http://www.sparkfun.com/products/245>
- [11] Corp., S. E. (n.d.). *Triple Axis Accelerometer Breakout-SCA3000*. Retrieved February 10, 2011, from Sparkfun Electronics: HYPERLINK "<http://www.sparkfun.com/products/8791>" <http://www.sparkfun.com/products/8791>
- [12] BIBLIOGRAPHY \l 1033 Torben Graversen, M. K. (2002). *Attitude Control system for AAU CubeSat* (http://www.cubesat.auc.dk/dokumenter/acs_report.pdf). 6: June.
- [13] BIBLIOGRAPHY \l 1033 BIBLIOGRAPHY Greg Welch, G. B. (2006, July 24). *An Introduction to the Kalman Filter*. Retrieved June 20, 2011, from The Kalman Filter: http://www.cs.unc.edu/~welch/media/pdf/kalman_intro.pdf

Inter-American University of Puerto Rico
Advance Research and Innovative Experience for students
(ARIES)

EQUIS Team 2011

Javier I. Espinosa Acevedo- Team Student Leader

Undergraduate Electrical Engineering, Male, Hispanic

Erika Portilla- Software Developer

Graduate Computer Science, Female, Hispanic

Jorge Quiñones Arduino- Calibration

Undergraduate Electrical Engineering, Male, Hispanic

Ana Espinal Mena- Attitude Determination System

Graduate Electrical Engineering, Female, Hispanic

Felix Rivera- Mechanical Structure Design

Graduate Mechanical Engineering, Male, Hispanic

Natacha Nazario – Project Manager

Undergraduate Aviation Manager, Female, Hispanic

Jose Almonte – Data Analysis

Graduate Computer Engineering, Male, Hispanic

Mairim Nieves – Attitude Determination

Undergraduate Electrical Engineering, Female, Hispanic

Inter-American University of Puerto Rico
Advance Research and Innovative Experience for students
(ARIES)

Introduction

EQUIS Mission Goal

The goal of this project is to develop an attitude determination systems (ADS) prototype, by improving the robustness and accuracy of a previous design (ABITA; Tiger team) in order to obtain relevant data and hands-on experience for a future satellite attitude control and determination system (ADCS). The designing, developing and testing will serve as a stepping stone for a future CubeSat project with the objective to transmit to a ground station the measurement data.

Science Objectives

- Obtain the platform body frame orientation with respect to the body fixed reference frame.
- To determine translation and attitude motion of the payload during flight.
- To measure the Earth's gravitational and magnetic field and the angular momentum of the payload such that the data can be used to determine the orientation of the payload.
- To measure the internal heat characteristic during flight and its potential impact on internal and structural components.

Technical Objectives

- Complete graphs and charts related to show the output of the different sensors as well as the translational and orientation motion of the cube.
- Develop a code to obtain data from the sensors and send it through telemetry.
- Use different attitude determination algorithms used to determine the attitude motion of the payload such as the Kalman Filter, to be used as the algorithms to determine the attitude motion.

Inter-American University of Puerto Rico
Advance Research and Innovative Experience for students
(ARIES)

HASP EQUIS Requirements

Fields	Design Requirements
Electrical	30 @ 500mA (Max)
	CubeSat PCB Size
Software	1200 Baud
Mechanical	3kg Weight Limit
Fields	Design Requirements
Electrical	30 @ 500mA (Max)

Data Preparation - Accelerometer (SCA3000)

To prepare for the data analysis the raw data needs to be calibrated and converted.

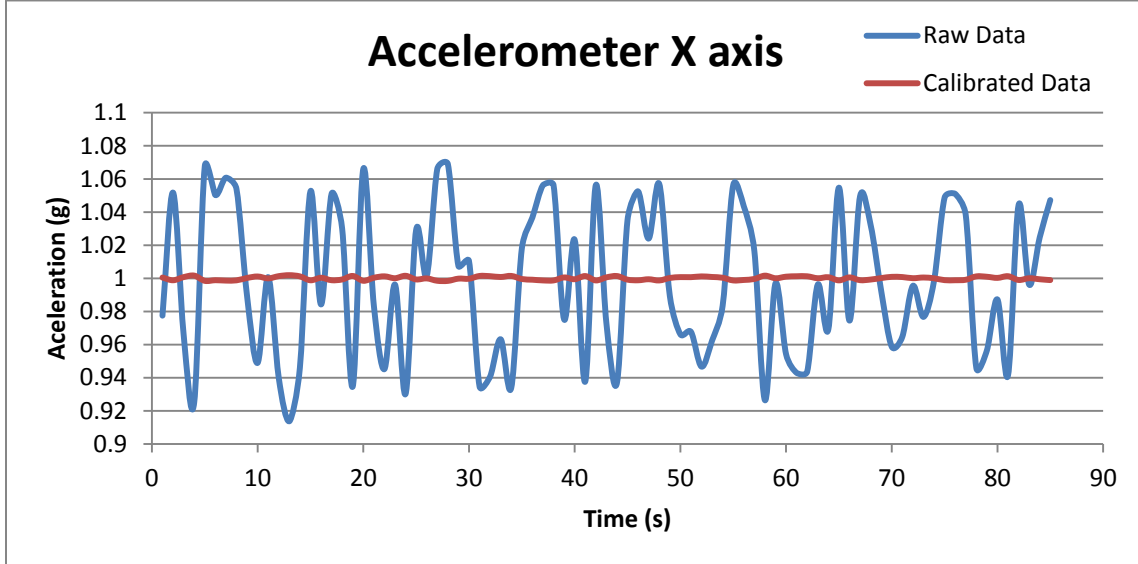


Figure 1: Accelerometer Raw and Calibrated Data X axis

Inter-American University of Puerto Rico
Advance Research and Innovative Experience for students
(ARIES)

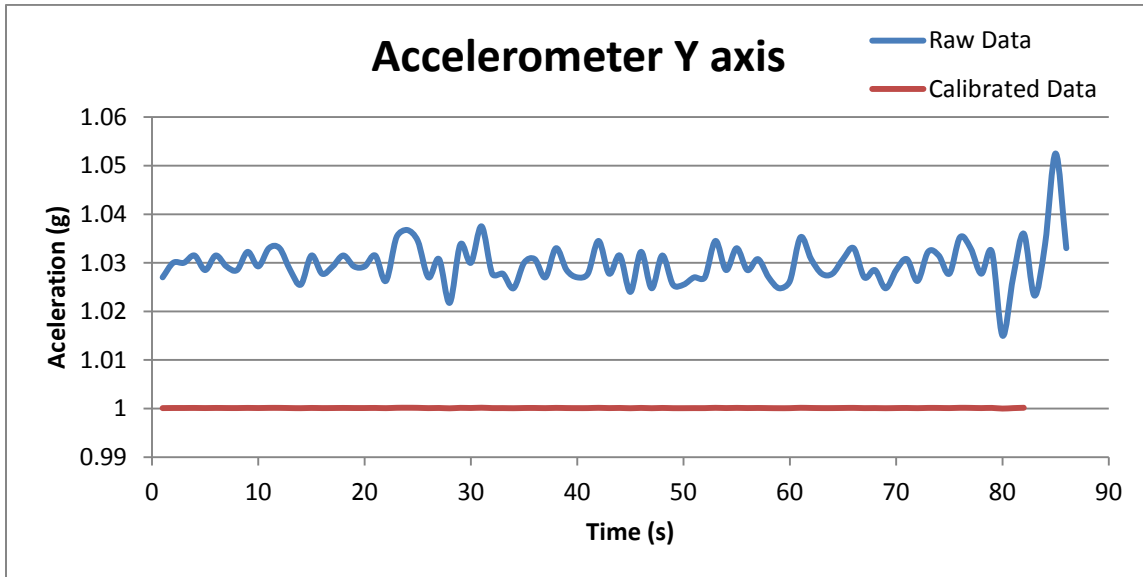


Figure 2: Accelerometer Raw and Calibrated Data Y axis

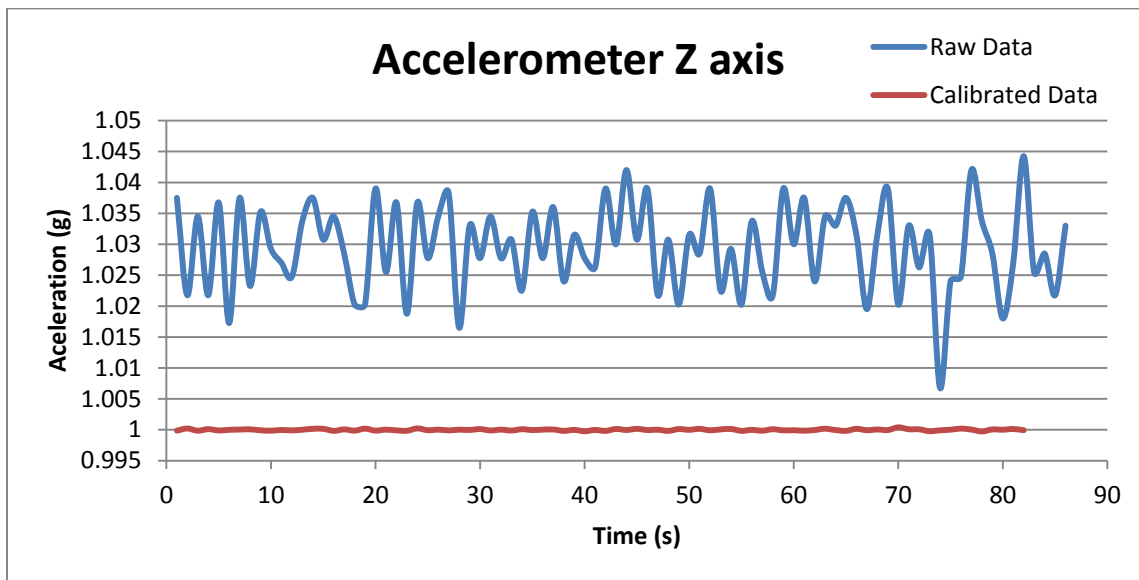


Figure 3: Accelerometer Raw and Calibrated Data Z axis

The accelerometer used was an SCA3000, it is a three axis sensor, the component needs to be calibrated to since the board and cube structure can cause errors. To analyze the data it is necessary to have the sensor calibrated and converted to real values to properly interpret the data. The data pass processed through a linear regression, then converted to real values and finally calibrated. Below is shown the process of this calibration:

Inter-American University of Puerto Rico
Advance Research and Innovative Experience for students
(ARIES)



Figure 4: Data Process for Calibration

The raw data is passed through a linear regression, and then converted to real values, finally calibrated (FR), this is done for all to analyze the data.

Data Preparation – Gyroscope

To prepare for the data analysis the raw data needs to be calibrated and converted.

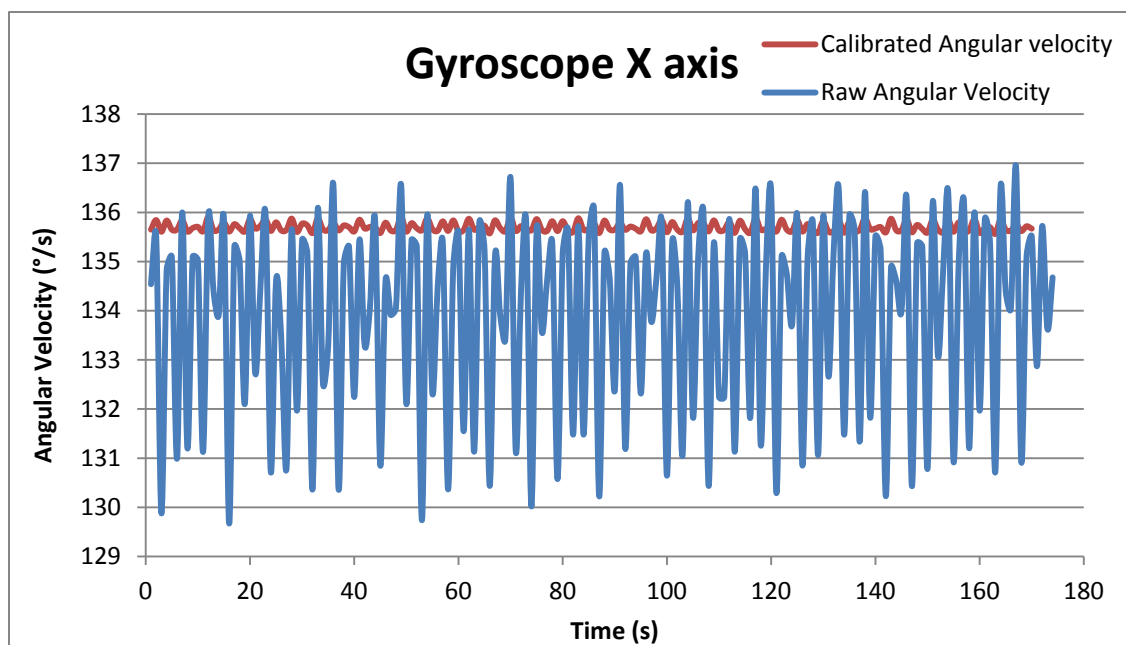


Figure 5: Gyroscope Raw and Calibrated Data X axis

Inter-American University of Puerto Rico
Advance Research and Innovative Experience for students
(ARIES)

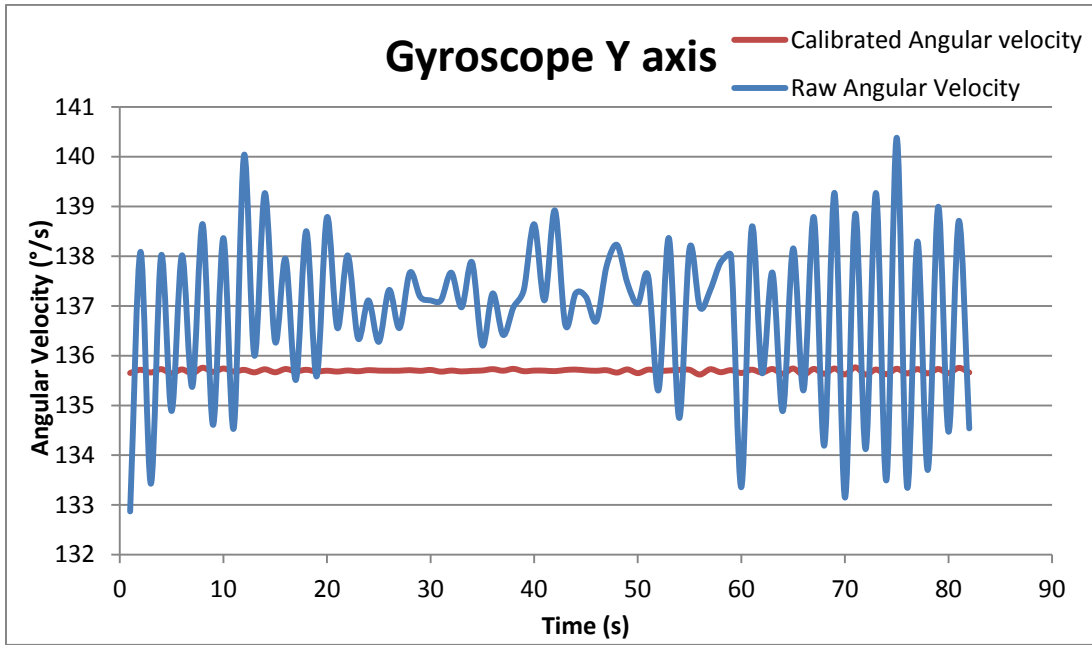


Figure 6: Gyroscope Raw and Calibrated Data Y axis

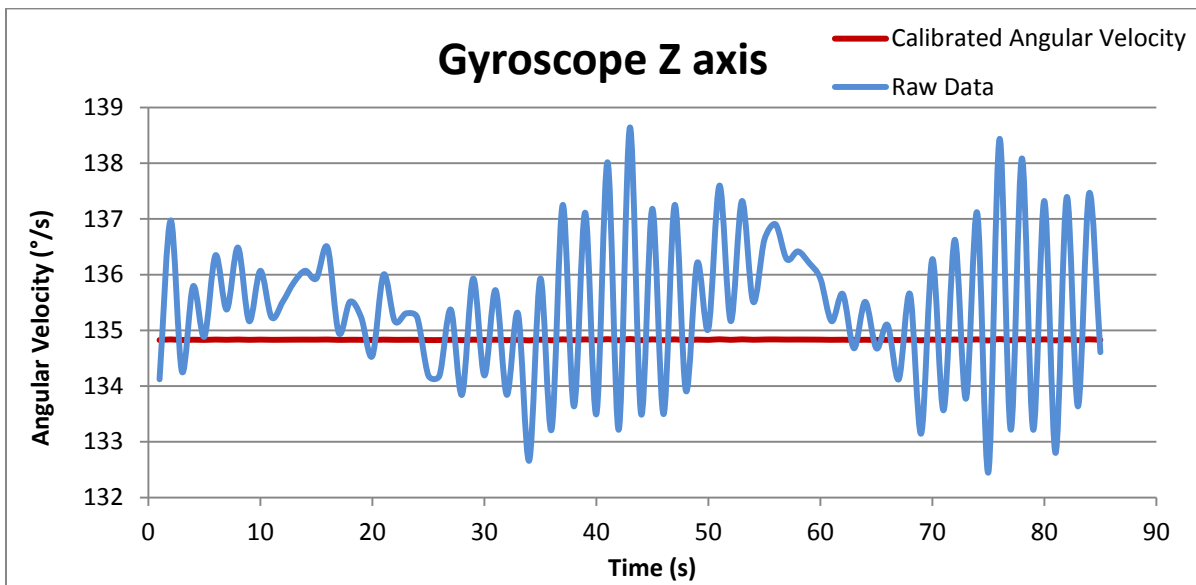


Figure 7: Gyroscope Raw and Calibrated Data Z axis

The gyroscope used was an ITG3200, it is a three axis sensor, the component needs to be calibrated to since the board and cube structure can cause errors. To analyze the data it is necessary to have the sensor calibrated and converted to real values to properly interpret the data. The data pass processed through a linear regression, then converted to real values and finally calibrated. Below is shown the process of this calibration:

Inter-American University of Puerto Rico
Advance Research and Innovative Experience for students
(ARIES)



Figure 8: Data Process for Calibration

The raw data is passed through a linear regression, and then converted to real values, finally calibrated (FR), this is done for all to analyze the data.

Calibration and Conversion Equations

$$\text{Accelerometer X Axis} = ((1.0032*(1.0030*(\text{RAW})-32.6208)/1333)+0.02066)$$

$$\text{Accelerometer Y Axis} = ((1.0278*(0.9826*(\text{RAW})+33.31)/1333)-0.0659)$$

$$\text{Accelerometer Z Axis} = ((1.0119*(0.9980*(\text{RAW}) -9.81211)/1333)-0.0243)$$

$$\text{Gyroscope X Axis} = ((1.0443*(0.9662439*(\text{RAW})-26.018)/14.375)+2.44732)$$

$$\text{Gyroscope Y Axis} = ((0.9744*(1.0212*(\text{RAW}) + 0.5418)/14.375)-0.561)$$

$$\text{Gyroscope Z Axis} = ((0.9962*(0.9896*(\text{RAW})+5.535)/14.375)-0.588447)$$

$$\text{Magnetometer X Axis} = ((0.997*(\text{B4})-52.865))/31.24$$

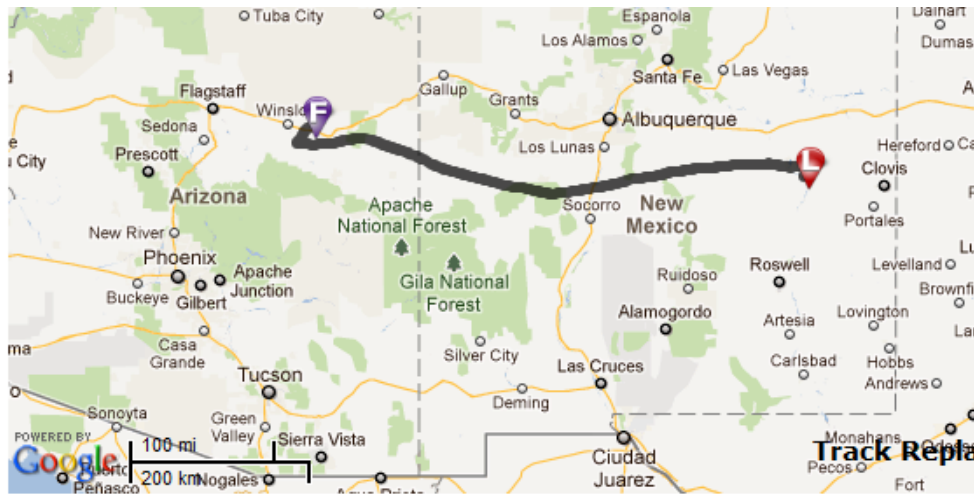
$$\text{Magnetometer Y Axis} = ((0.997*(\text{B183})-52.865))/31.24$$

$$\text{Magnetometer Z Axis} = ((1.000015*(\text{D5})-101.32))/31.24$$

Inter-American University of Puerto Rico
Advance Research and Innovative Experience for students
(ARIES)

Flight Analysis

Through the LSU HASP site it was possible to obtain the image in **Figure 9**, it is possible to observe that the Zero Pressure Balloon started in New Mexico and ended Arizona. During this time many data was obtained, therefore the data will be divided into phases to amplify the resolution in the charts.



Current HASP Position

Time: 09/01/11 00:28:04 GMT MET: 11.37 hours
Lat: 35.0059 deg Lon: -110.4052 deg Alt: 5216 ft
Heading: 0.0 deg SOG: 17.1 knots Horizon: 88.44 miles
Distance Over Ground: 353.40 miles Total Flight Distance: 410.28 miles

Figure 9: Complete flight path HASP 2010 (Sept 31, 2011)

The data will be divided into two phases: Phase 1 **Elevation** and Phase 2 **Flight** as shown in **Figure 10**. The division of the phases of the flight will allow better analysis because data resolution will be higher. Phase 1 starts from the launch to the point that the altitude from the GPS data is not incrementing drastically (Reaches approx. 120,000ft) this phase is approximately 2-2 1/2hrs and has faster dynamics and turbulence. Phase 2 starts right after phase 1 and last until the rest of the flight, this phase has slower and smoother dynamics.

Inter-American University of Puerto Rico
Advance Research and Innovative Experience for students
(ARIES)

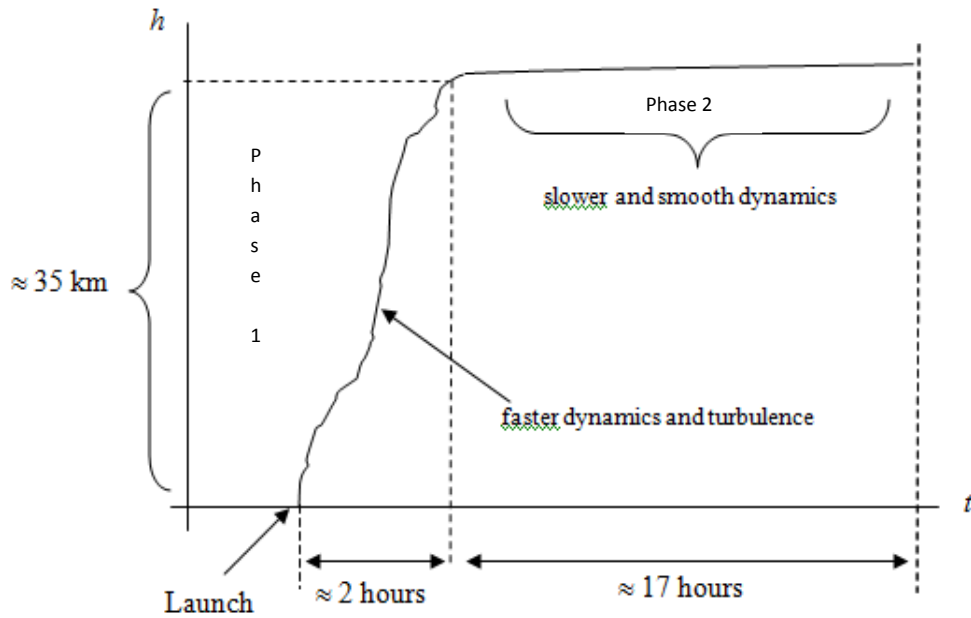


Figure 10: Flight Dynamics division by phases

Phase 1

In Figure 11 it can be observed the path taken during the Phase 1. At 15:48:54 GMT on September 31, 2011, 2.72 hours after launch it reached an altitude of 123595 ft. Therefore after 2 hours and 43 minutes it had reached this altitude, the time recorded on the payload started at 8:22, meaning that phase 1 will end at 11:05 according to the real time clock on the payload.



Figure 11: Phase one flight path of approx. 2.72 hours

Inter-American University of Puerto Rico
Advance Research and Innovative Experience for students
(ARIES)

Phase 1 Accelerometer

Through the SCA3000 it was possible to able to obtain the acceleration of the payload through the flight. During the first 2.75hr of flight the data obtained was plotted in the **Figure 12**.

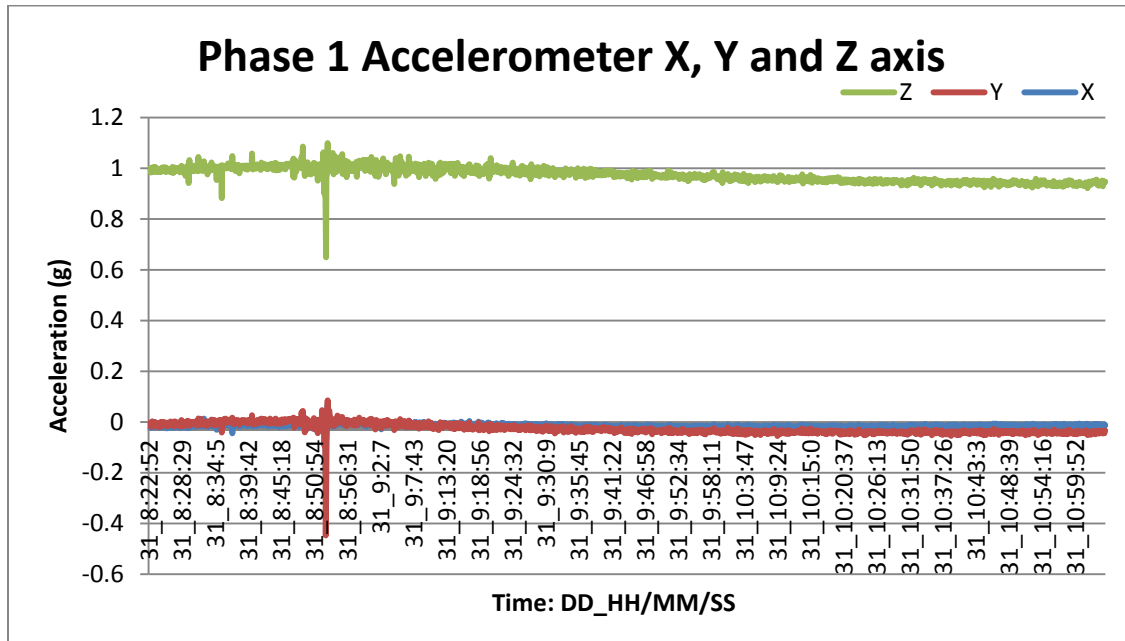


Figure 12: Payload Acceleration in three axis during phase 1

Observing the graph it is possible to notice that during flight the intensity of the acceleration maintained at approx. 1g of gravitational force. Also a significant increase in acceleration was measured by all three axis at approximately 30min after flight this could represent noise of the sensor. The z axis was pointing in the vertical direction and the other two axis where perpendicular to the Z axis, therefore it expected that the z axis will be the component with most magnitude. Accordingly during the first phase there were no fast dynamics.

Phase 1 Gyroscope

The gyroscope sensor will give the rotational rate of the payload during the flight in three axes, the z axis is in the vertical direction. Accordingly to the data of the phase 1 plotted in **Figure 12** it is possible to observe that in the y axis the gyroscope was rotating at a slow and increasing rate of approximately of fifteen degrees per second during the first hour and then paused and started reducing at approximately the same rate until the payload reached a negative (counter clockwise) rotational rate of approximately 12 °/s. The Y axis has a similar behavior of that of the Y axis, it is possible notice that a maximum of approx. 10°/s in the clockwise direction and 7 °/s in the CCW direction was obtained. The X axis reached a CW rotational rate of 5 °/s max and a CCW

Inter-American University of Puerto Rico
 Advance Research and Innovative Experience for students
 (ARIES)

rate of 6 %/s. During the first hour and fourteen minutes the HASP payload rotated CW approximately 88 rotations (360°), therefore in the first 74 min the payload rotated $428^\circ/\text{min}$ in other words an average rotational rate of 1.2 rotations per min.

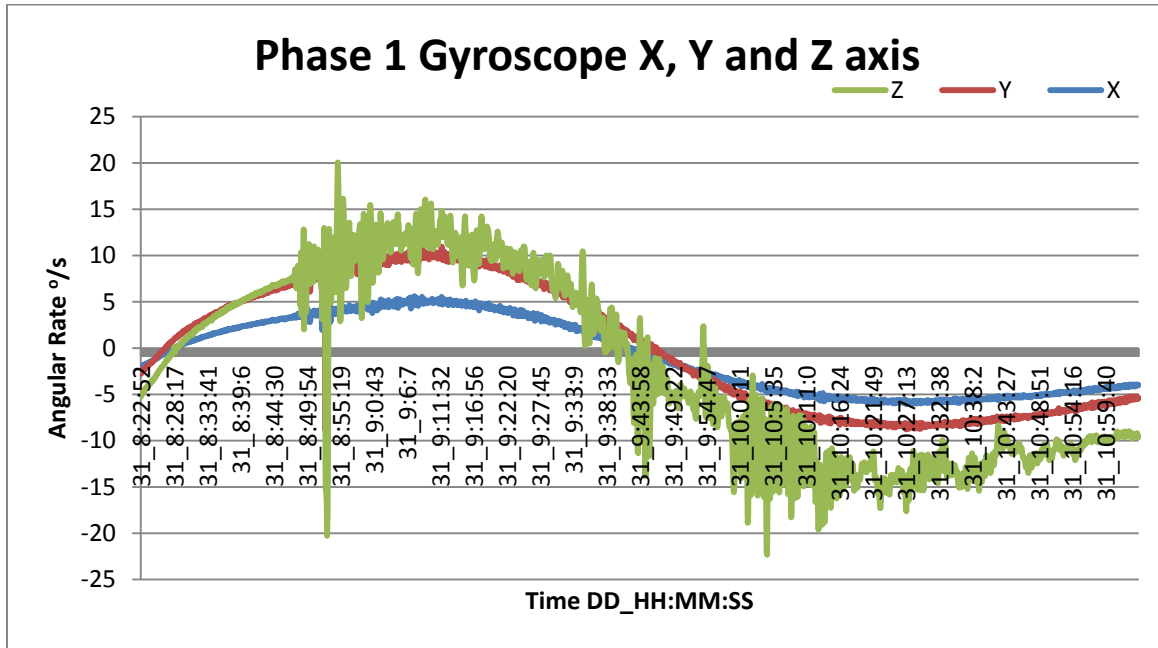


Figure 13: Phase 1 Gyroscope Data

Phase 1 Magnetometer

Data analysis using the magnetic field can become very complex, the magnetic field properties of the earth are in a constant change. In Figure 14-16 it is possible to observe the magnitude recorded on each axis of the Micromag3 sensor during phase I of the flight. It is possible to observe that in the x axis the magnitude recorded varied from -25uT to 23uT. The Y axis varied from -32uT to 18uT and the Z axis remained fairly constant approximately 39.17uT.

Inter-American University of Puerto Rico
Advance Research and Innovative Experience for students
(ARIES)

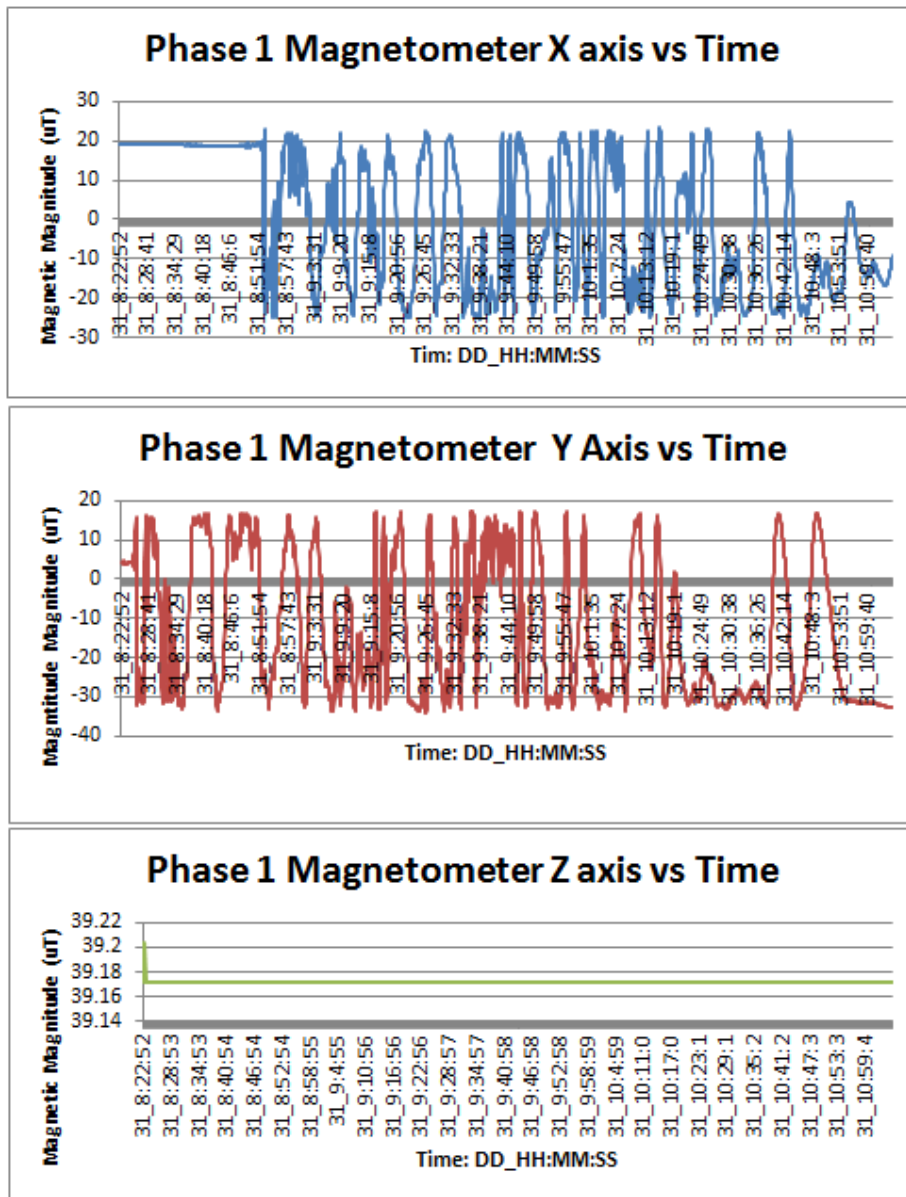


Figure 14: Magnetic Magnitude in X, Y and Z axis

Observing the data it can be possible to understand the resolution and range of the data; therefore, through the data analysis it could be possible to determine if the sensor would be appropriate for an attitude determination system. To understand the data it was converted to field intensities (F) with **Equation 1**.

$$\text{Equation 1: } F = \sqrt{X^2 + Y^2 + Z^2}$$

Where:

F: Total Field Intensity

Inter-American University of Puerto Rico
Advance Research and Innovative Experience for students
(ARIES)

X: x axis of magnetometer
Y: y axis of magnetometer
Z: z axis of magnetometer

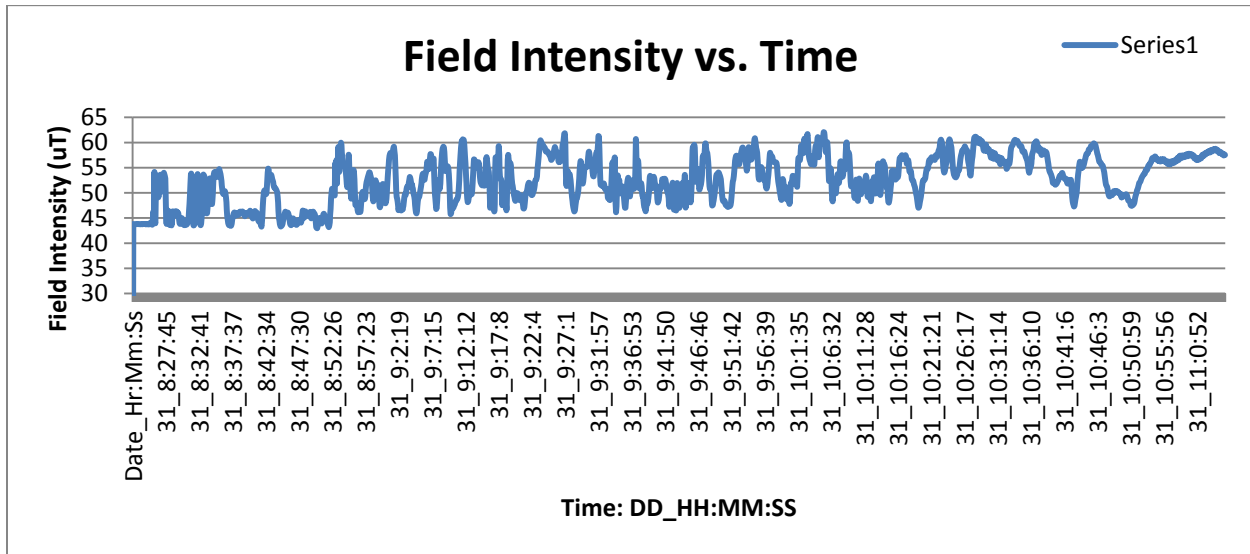


Figure 15: Field Intensity vs Time during Phase 1

The **Figure 15** permits an understanding that the field intensity was in the range of 44 to 61uT. Since we know it was in the United States where the flight took place it is possible to observe that the payload headed north during the flight to some degree. In **Figure 16** it is possible to observe the earth magnetic field intensity over the US, it can be observed that the field intensity increases more in the north direction. A small square represents where New Mexico will be located on the map, permitting to identify the field intensities of the area.

Inter-American University of Puerto Rico
 Advance Research and Innovative Experience for students
 (ARIES)

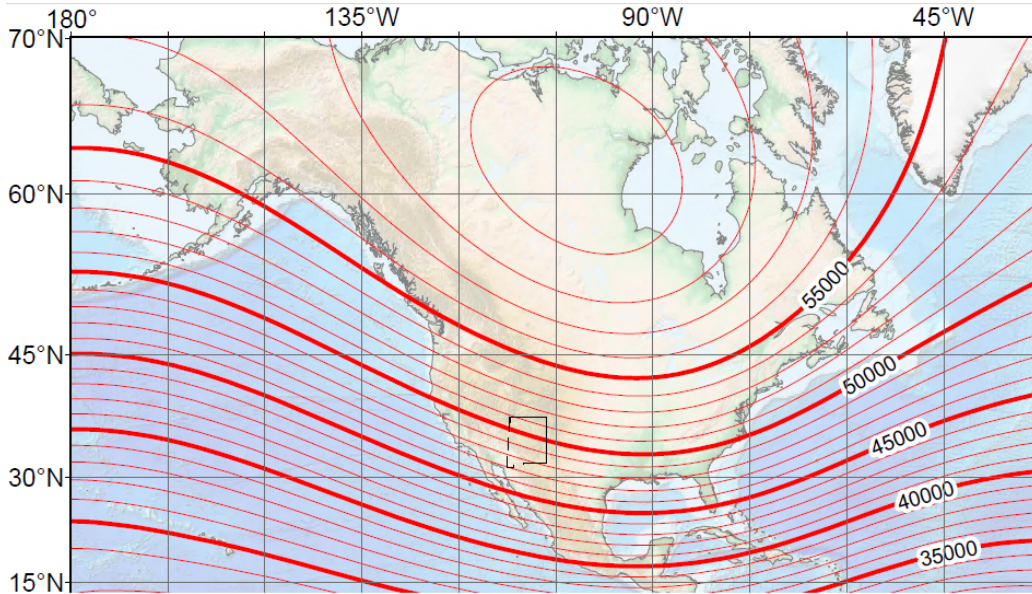


Figure 16: 2010 Magnetic Field Intensity [2]

Phase 1: Internal Temperature

During the first phase of the flight the internal temperature varied, it first went from 16°C to 37°C then it slowly decreased to a value of 2°C. The phase one finished with a temperature of 7°C. Allowing us to acknowledge that the internal temperature in the payload remained within the establish parameters.

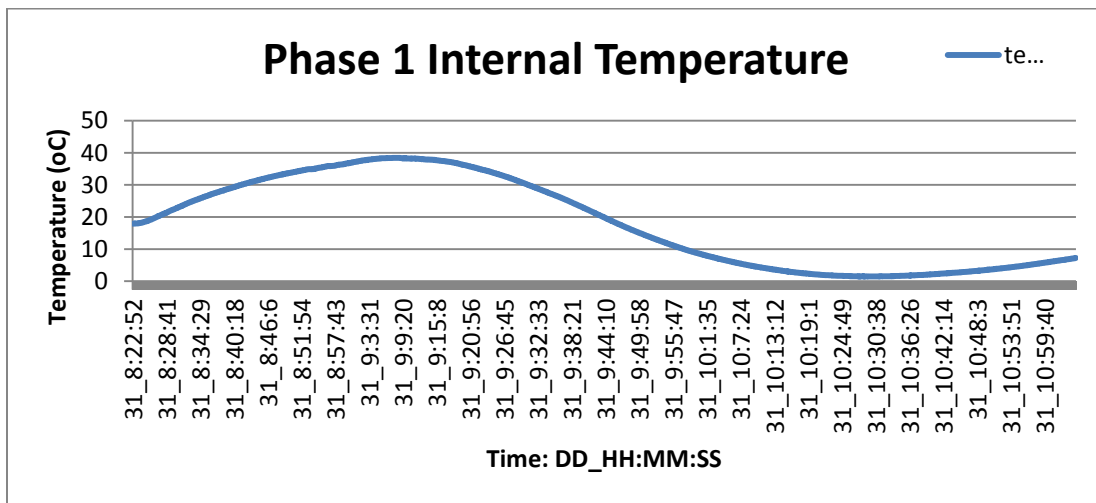


Figure 17: Temperature Profile during phase I

Inter-American University of Puerto Rico
Advance Research and Innovative Experience for students
(ARIES)

Phase II

The phase is the longest section of the flight it lasts approximately hrs, in Figure 18 it can be observe the location of where the first phase ended and where phase II started. This phase finishes where the payload reaches its final location mark with the purple “F” located in Arizona.



Figure 18: EQUIS 2011 Complete Flight Trajectory

Phase II Accelerometer

It was possible to able to obtain the acceleration of the payload through the period of the flight. During this phase 7:36hrs of flight data was obtained and plotted in the **Figure 19**. In the plot we have all three axis, it can be observe that the accelerometer measured 1g (earth’s gravitational acceleration) in the Z axis and closely to zero the Y and X axis. This is known to be true since the Z axis is in the vertical direction. Comparing **Figure 19** with **Figure 12** it can be observed that phase II had obtain less acceleration, even though they are very similar. 1G is the earth’s gravitational acceleration.

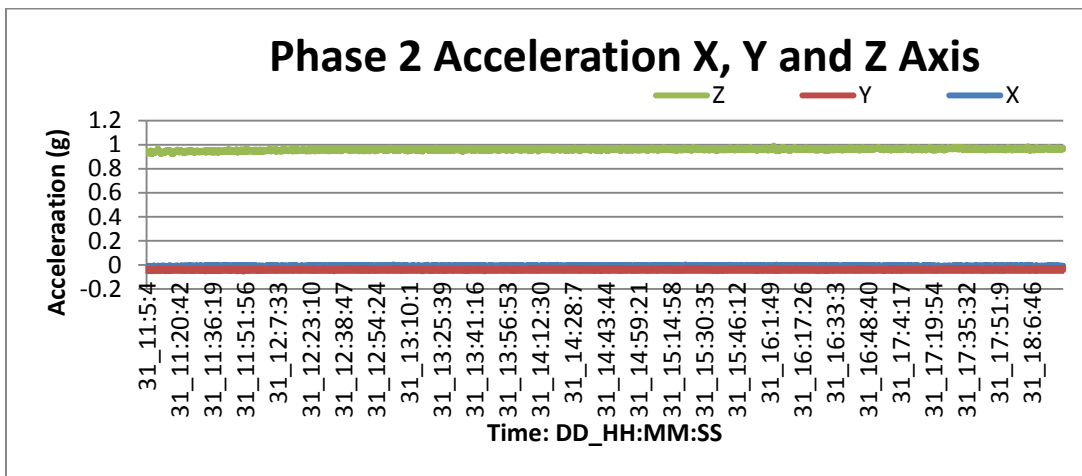


Figure 19: Phase II Acceleration vs Time

Inter-American University of Puerto Rico
Advance Research and Innovative Experience for students
(ARIES)

Phase II Gyroscope

During the phase II, by observing **Figure 20**, it is possible to notice that the rotational rate varied from $-10^{\circ}/s$ to $+7^{\circ}/s$. By using approximations it is possible to know how many rotations (360°) the payload has given during a time period. We can observe that from 12:04 to 18:19 the payload gave approximately 258 rotations in the CW direction. Therefore in phase there were more rotation in the CW direction at an average rate of approximately 5 degrees per second after time 12:04.

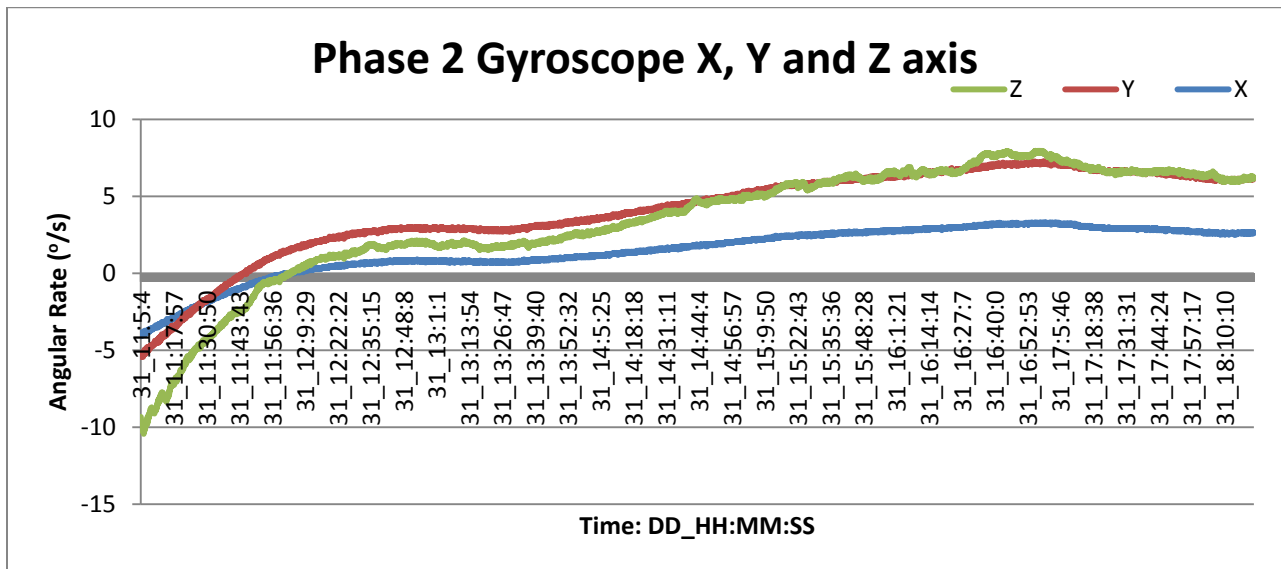


Figure 20: Phase II Rotational Rate vs time

Phase II Magnetometer

In **Figure 21** the variations of the magnetic field were in the same range of that in **Figure 14** of Phase I. In comparison with phase 1 the variations were much less in the phase II of the flight. The magnitudes obtained are converted to Field Intensity of allow a better understanding of the data.

Inter-American University of Puerto Rico
 Advance Research and Innovative Experience for students
 (ARIES)

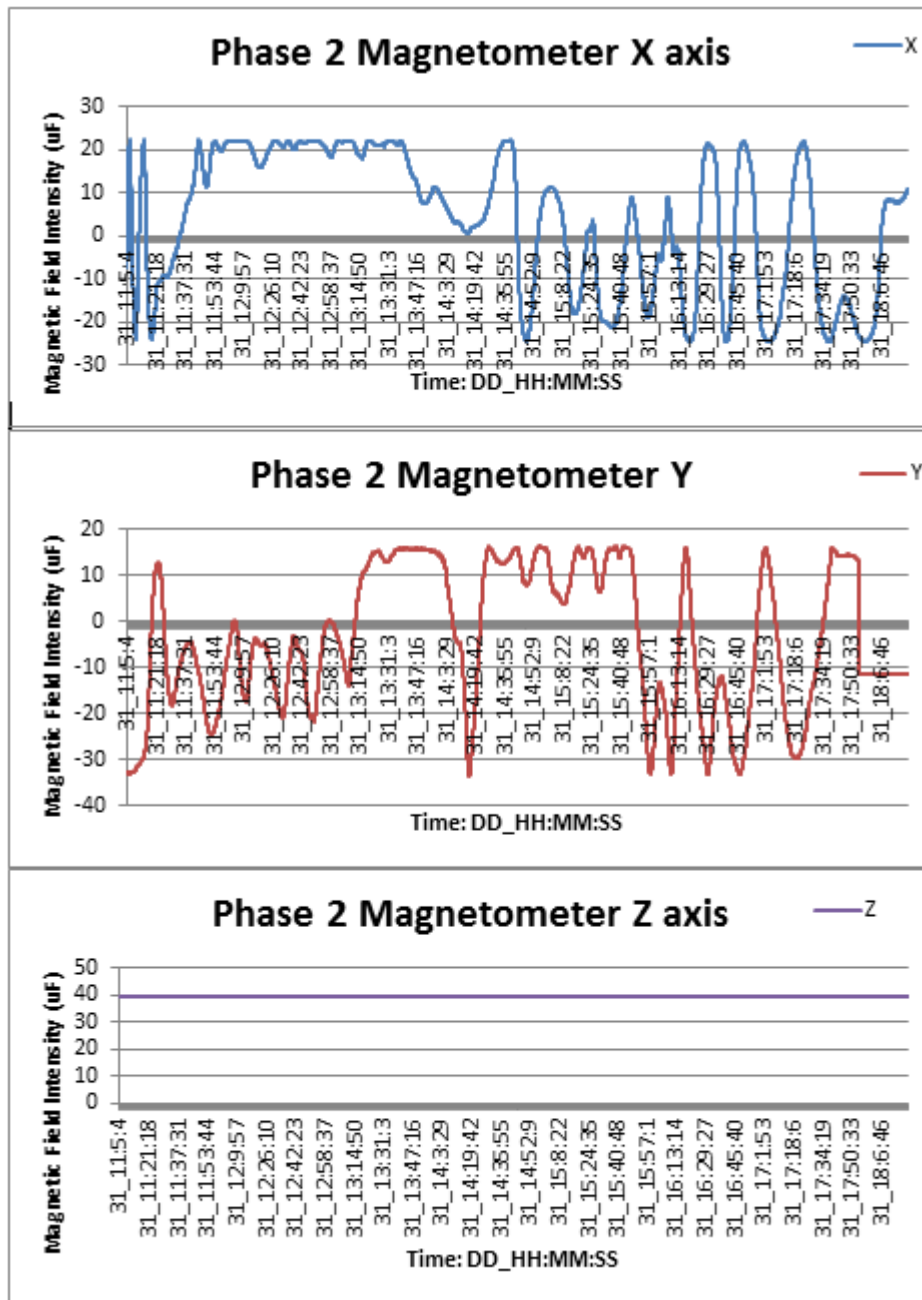


Figure 21: Magnetic Magnitude in X, Y and Z axis

Inter-American University of Puerto Rico
 Advance Research and Innovative Experience for students
 (ARIES)

With Equation 1 shown again for convenience

$$F = \sqrt{X^2 + Y^2 + Z^2}$$

It is possible to observe the field intensity variation throughout the flight in **Figure 22** the variation were in the range of 61uT to 49uT, this can allow us to identify more area where the payload was exposed to, all through the values are greater than that of the Figure 16. This could be caused by Electromagnetic Interference by the other payloads.

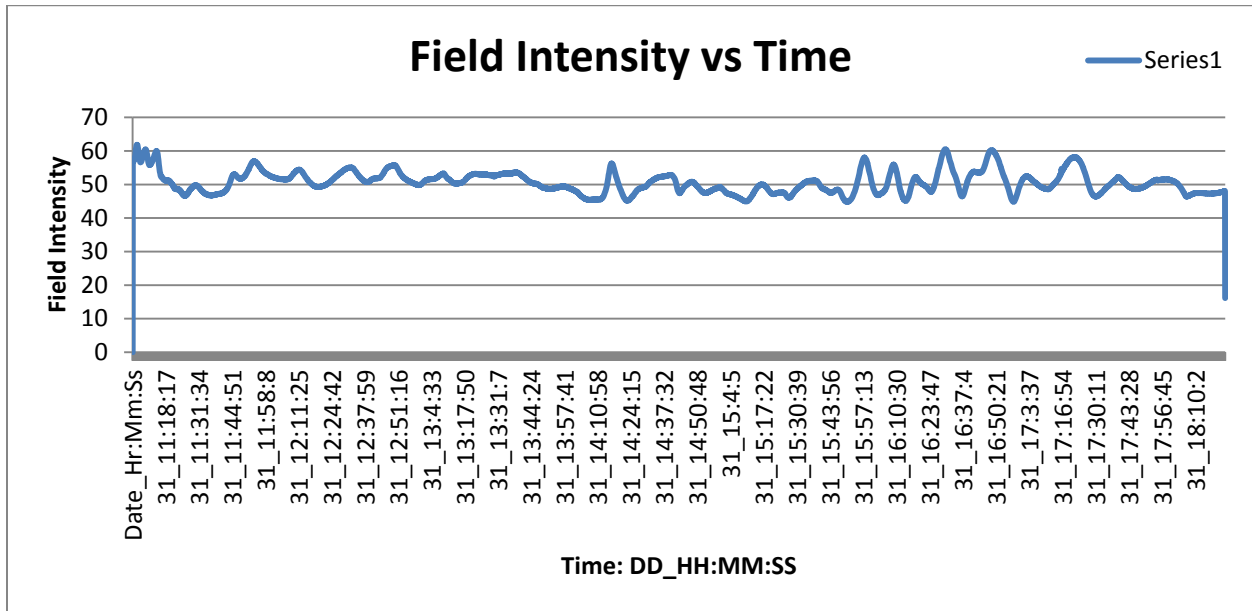


Figure 22: Field Intensity vs Time

Inter-American University of Puerto Rico
Advance Research and Innovative Experience for students
(ARIES)

Attitude Determination (Kinematic Equations)

The attitude determination system will be using the accelerometer, magnetometer and gyroscope data to perform a calculation which will describe the rotation and orientation of the platform during flight. For instance, let us use the gyroscope data to describe the angular velocity. The following kinematic equation describes the rotation of the body about its center of mass. This equation is described in terms of the quaternion and angular velocity. The angular velocity is obtained from an IMU located in the body of the HASP payload. The kinematic equation can be written as,

$$\frac{dq}{dt} = \begin{bmatrix} 0 & -\omega_1 & -\omega_2 & -\omega_3 \\ \omega_1 & 0 & \omega_3 & -\omega_2 \\ \omega_2 & -\omega_3 & 0 & -\omega_1 \\ \omega_3 & \omega_2 & \omega_1 & 0 \end{bmatrix} \begin{bmatrix} q_1 \\ q_2 \\ q_3 \\ q_4 \end{bmatrix} \quad (1)$$

where $\vec{\omega}$ is the angular velocity of the body, and $q = \vec{q} + q_4$. q is the quaternion explaining the orientation of the HASP platform, and q_4 is the magnitude of the rotation of the body. The calibrated data of the gyroscope for the HASP 2010 payload was substituted into equation (1), and it is assumed that the initial quaternion is,

$$q_0 = 0\hat{i} + 0\hat{j} + 0\hat{k} + 1$$

A quaternion is a four component object with a three vector part and a scalar part. For this case the scalar part is 1. The quaternions are used instead of Euler angles to represent rotation due to the simplicity of calculation. In addition they are simpler to compose and avoid the problem of gimbal lock.

Using a MatLab code to integrate equation (1) with a real data taken from HASP 2010 in **Figure 24** and **Figure 25** shows the quaternion components obtained from the integration procedure.

Inter-American University of Puerto Rico
Advance Research and Innovative Experience for students
(ARIES)

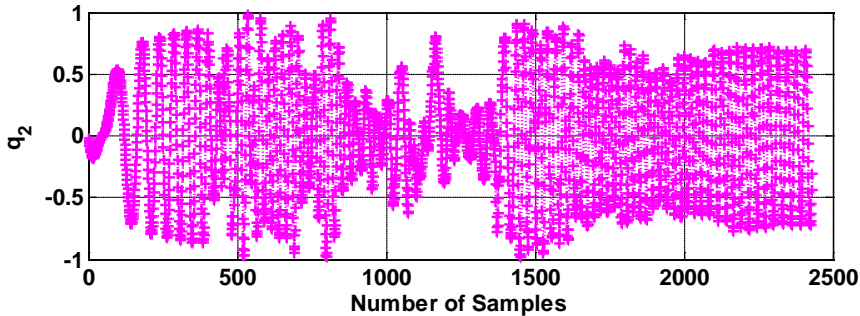
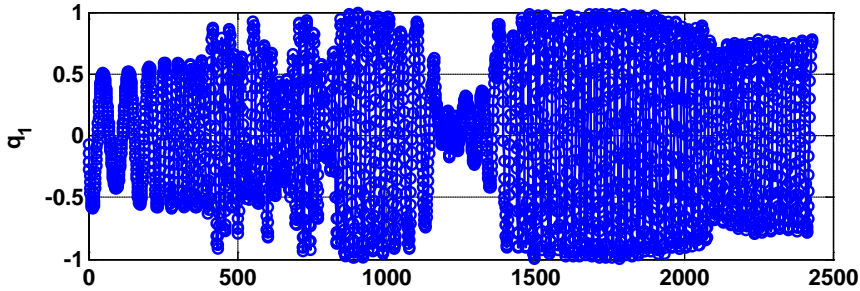


Figure 23: q_1 and q_2 of the quaternion components of HASP 2010

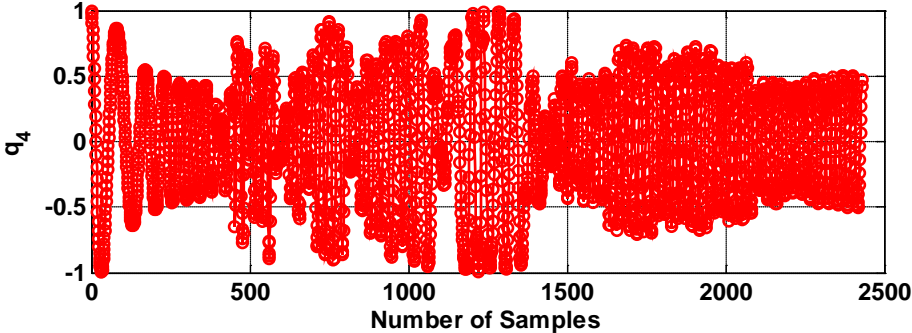
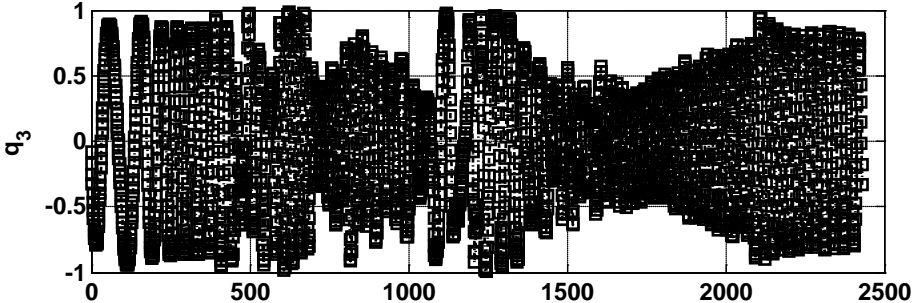


Figure 24: q_3 and q_4 of the quaternion components of HASP 2010

Inter-American University of Puerto Rico
Advance Research and Innovative Experience for students
(ARIES)

Figure 24 and **Figure 25** shows a normalized quaternion. This is due each time is converted from Euler Angles to quaternion and in reverse operation is added some error to the result. Furthermore, is necessary to normalized the result each time this operation is performed.

After is performed the rotation using quaternion is then transformed into Euler Angles. The Euler angles provide a better understanding of the satellite motion. The transformation from quaternion into Euler angles can be written as,

$$\sin \theta = 2q_4q_2 - 2q_1q_3 \quad (2a)$$

$$\tan \varphi = \frac{2q_2q_3 + 2q_4q_1}{2q_4^2 + 2q_3^2 - 1} \quad (2b)$$

$$\tan \psi = \frac{2q_1q_2 + 2q_4q_3}{2q_4^2 + 2q_1^2 - 1} \quad (2c)$$

θ is the pitch angle, φ is the roll angle, and ψ is the yaw angle. The roll, pitch, and yaw angles describes the rotation about the x, y, and z axis of the payload, respectively. Using these equations, Figure 26 shows the angle motion of the payload. In Figure 26, the yaw angle shows that the payload base was rotating from -90 to 90 degrees about the z axis. The roll motion shows a very similar rotation, but there is a point in time that the payload is close to 10 degrees. This means that the wind is causing the base to rotate a lot about the x and z axis while the y axis shows a bounded motion. This data provides insight into the platform motion and allows the development of the following payload. However, for the pitch axis is where was rotating less comparing with the range of motion the platform had.

Inter-American University of Puerto Rico
Advance Research and Innovative Experience for students
(ARIES)

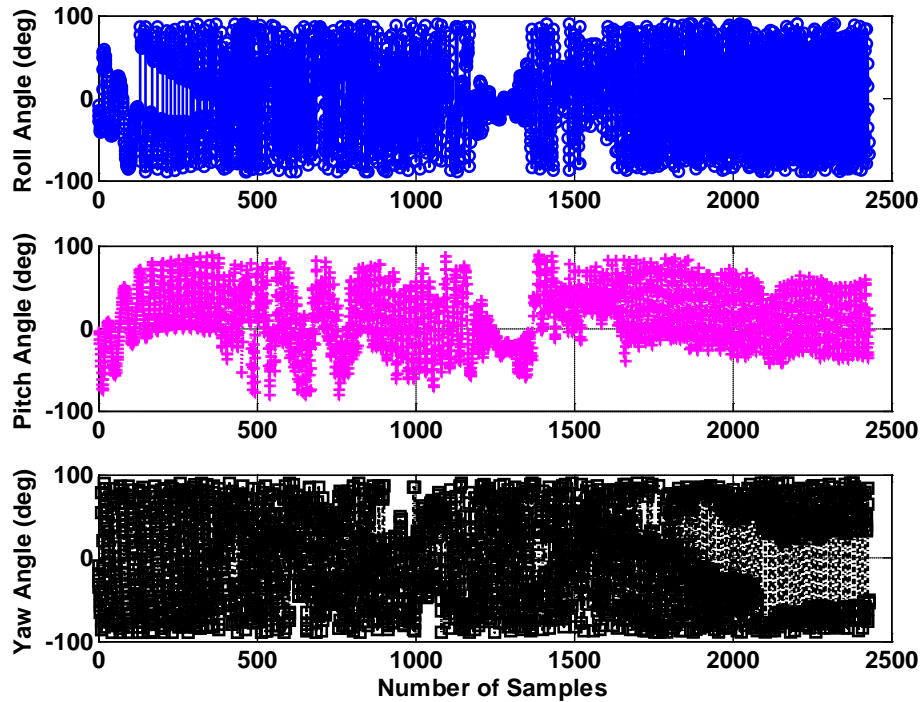


Figure 25: Euler angles for data of HASP 2010

The Kalman filter is an algorithm which uses a system dynamic model used to process noisy data retrieved from sensors measurements as an example, to accurately predict an attitude motion of an object in movement. It use a recursive mathematical model to estimate the state of a process while minimizing any error in the system. The purpose is to force the measured and estimated values for the filter's state to converge and for the difference between the estimate and actual state, to be minimized. The Kalman filter can be represented by the following equation,

$$\bar{X}_k = K_k Z_k + (1 - K_k) \bar{X}_{k-1} \quad (3)$$

where,

$$\begin{aligned} \bar{X}_k &= \text{current estimation} \\ K_k &= \text{Kalman gain} \\ Z_k &= \text{measured value} \\ \bar{X}_{k-1} &= \text{previous estimation} \end{aligned}$$

and the k subscript are states or in state vectors,

$$x(k) = Ax(k - 1) + Bu(k - 1) \quad P(k) = AP(k - 1)A' + Q$$

where P is the initial value of covariance and Q is the process noise covariance.

Kalman Filter Mechanics

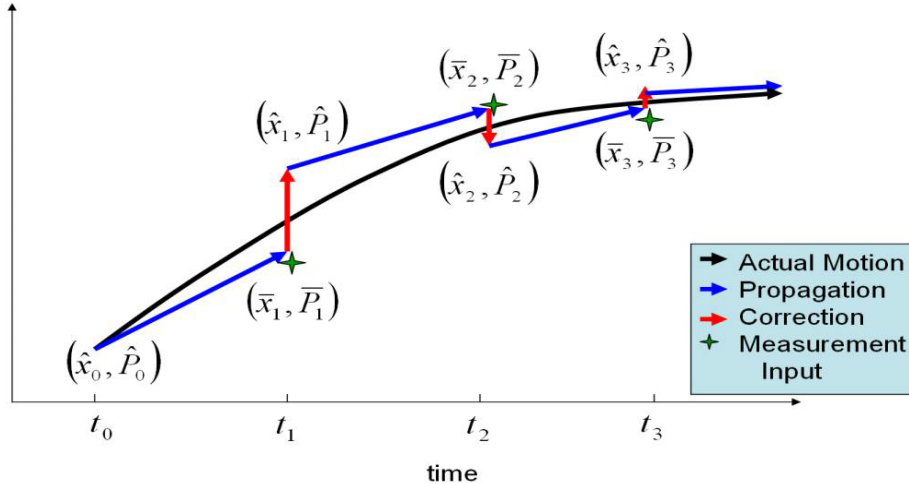


Figure 26: Kalman Filter process for converging on a true state vector

Figure 27 shows a graph representation of what the Kalman Filter perform. The y-axis represent the position and the x-axis the time. Each new step will try to correct its error using the previous value. The Kalman Filter can be used together with the Gauss-Newton method. The Gauss-Newton method is used to solve non-linear least squares problems. This method uses $B_k = J_k^T J_k$ where J_k is the Jacobian matrix. Its advantage is that for a second derivative which can be difficult to compute is not required.

Using the data from HASP 2010 was implemented the Kalman Filter as shown in **Figure 28** and **Figure 29**.

Inter-American University of Puerto Rico
Advance Research and Innovative Experience for students
(ARIES)

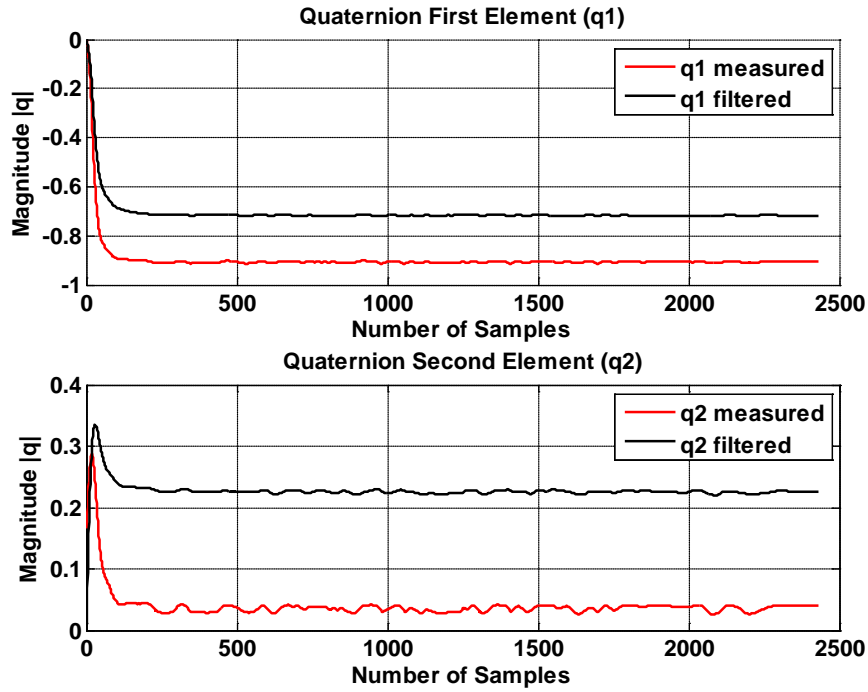


Figure 27: q1 and q2 of the filtered quaternion components of HASP 2010

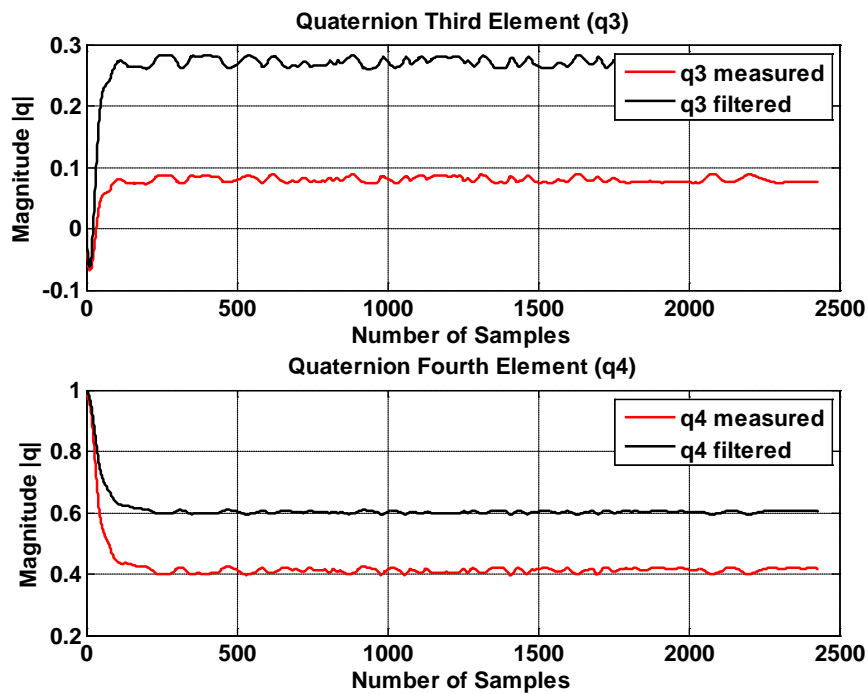


Figure 29 q3 and q4 of the filtered quaternion components of HASP 2010

Inter-American University of Puerto Rico
Advance Research and Innovative Experience for students
(ARIES)

If is compared **Figure 28** and **Figure 29** using the quaternion after using the algorithm of the Kalman Filter, exists some difference between the phase of q_1 and q_2 . This indicates an opposite direction for rotation about these axes. Also there is some bias for the measured and filtered values of the quaternion. This is due because most of the gyroscope has a bias offset also known as the null voltage and is the measured voltage when the gyro is not rotating about its axis. The gyro output voltage measurements above the bias offset indicate rotation in one direction, while voltage measurements below the bias offset indicate rotation in the opposite direction.

Figure 30 shows the output when is transformed from the quaternion back to Euler Angles. For the data of HASP 2010 is noticed that looking on the Euler Angles it present more stabilization for the roll axis. However, at some sample number about 70-80 occurred a drastic change of motion for the roll, which did not occur for the smooth transition at the start for pitch and yaw.

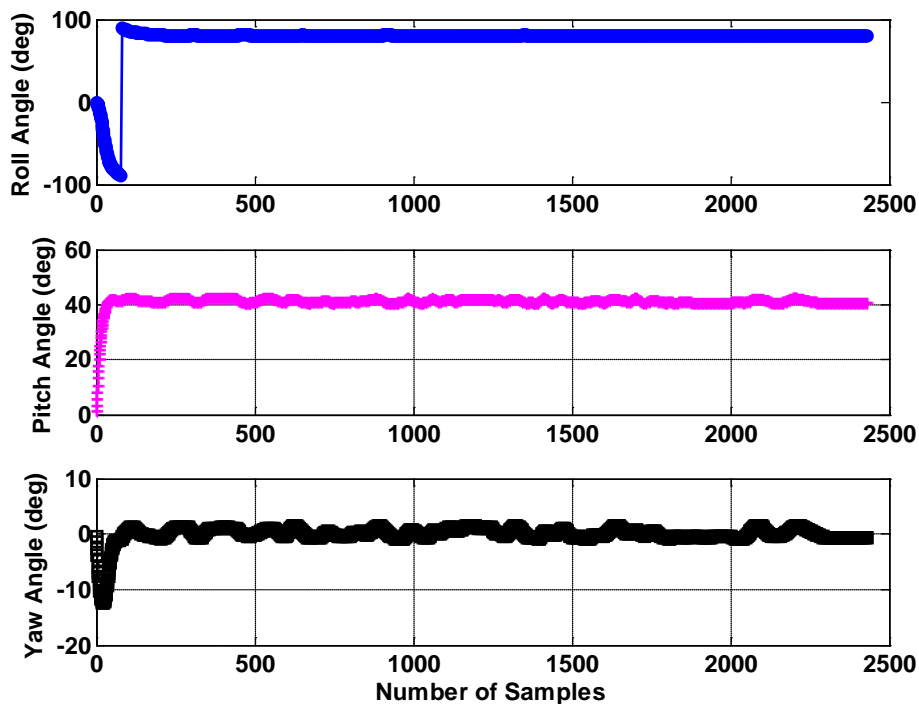


Figure 28: Euler Angles in for x, y and z axes of HASP 2010

Inter-American University of Puerto Rico
Advance Research and Innovative Experience for students
(ARIES)

Conclusion

The development of this payload allowed us to learn about the development of a payload that can be flown on a zero pressure balloon. This was a process of going through Pre PDR, PDR, Pre CDR, CDR, FRR, Integration Plan, FLOP and Final Report. This process was learned at the Louisiana State University through the High Altitude Student Platform, with meetings with Dr. Guzik's panel. The implementation of an attitude determination system was completed, tested and flown on September 2011. After flight it was possible to analyze the data in a graphical format and obtains the characteristic of the behavior of the EQUIS payload through the Attitude Determination System (ADS), thus allowing us to observe the range of the data, the resolution and variations throughout the flight. It is necessary to understand that a graphical analysis can help understand the behavior of the payload throughout the flight. It was possible to notice through the data that phase I had faster dynamics and that the phase II was slower, as expected.

The measurements of the Earth's magnetic field, gravitational field and angular momentum from the IMU sensors, which consisted of accelerometer, magnetometer, and gyroscope were successfully determined and transformed to quaternions to obtain the orientation and attitude of the payload. After implementing the Kalman filter algorithm in the quaternions, it resulted in a signal with lower noise and higher precision, thus increasing the reliability of our attitude estimation. These quaternions were transformed to Euler angles consisting of roll, pitch, and yaw angles and the results showed that the transition from Euler angles to quaternion did not affect the final results. When comparing the motion in roll, pitch, and yaw, the roll motion shows a very similar rotation, but there is a point in time that the payload is close to 10 degrees. This means that the wind is causing the base to rotate a lot about the x and z axis while the y axis shows a bounded motion.

Inter-American University of Puerto Rico
Advance Research and Innovative Experience for students
(ARIES)

Appendix A: Calibration Procedure

This section it explained in details the device used, procedures for calibration, calibrations equations and a comparison between the not calibrated data vs. the calibrated data.

**Report Document
for the
High Accuracy Calibration Mechanism for
Attitude Determination Systems**

Prepared by:

Team Spokesperson (Jorge J. Quiñones) Date

Team Member (Javier Espinosa) Date

Revised:

Inter-American University of Puerto Rico
Advance Research and Innovative Experience for students
(ARIES)

Approved:

Institution Signoff (Dr. Hien Vo)

Date

TABLE OF CONTENTS

Cover.....
Table of Contents
1.0 Document Purpose	2-3
1.1 Document Scope.....	2
1.2 Change Control and Update Procedures.....	3
2.0 Reference Documents	3-4
3.0 Tables of Figures.....	5
4.0 Calibration Procedure	6-14
4.1 Calibration Procedure.....	6-14
4.1.1 Accelerometer.....	8-9
4.1.2 Gyroscope.....	10-11
4.1.3 Magnetometer.....	12-13
4.2 Calibration Results.....	15-20
5.0 Acknowledgments.....	21
6.0 Glossary	22

Inter-American University of Puerto Rico
Advance Research and Innovative Experience for students
(ARIES)

1.0 Document Purpose

This document describes the process of calibration using the High Accuracy Calibration Mechanism for Attitude Determination Systems.

1.1 Document Scope

This document specifies the Calibration of the sensors currently used on the HASP 2010 payload also provides the results of the calibration procedure. The document includes details of the calibration equations, procedure, performance, implementation and software development.

1.2 Change Control and Update Procedures

Changes to this document shall only be made after approval by designated representatives from High Accuracy Calibration Mechanism for Attitude Determination Systems and the ARIES Institution Representative.

2.0 Reference Documents

Al-Nasir, J. (n.d.). *How does INS work?* Retrieved from http://www.al-nasir.com/www/Jamie/Articles/Technology/INS_Inertial_Navigation_explained.shtml

How Does an Accelerometer Work? (2011). Retrieved March 2011, from EzineArticles.com: <http://ezinearticles.com/?How-does-an-Accelerometer-Work?&id=285604>

Blue Point Engineering. (2007). *Servo Information*. Retrieved from <http://www.bpesolutions.com/bpemanuals/Servo.Info.pdf>

Central School for Tibetans. (2007). Retrieved from <http://cstdalumni.org/invision-utilitech-3-non-ic-white-gimbal-recessed-kit/>

CNCroutersource. (2007). *Open vs. Closed loop system*. Retrieved 2001, from <http://www.cncroutersource.com/closed-loop-system.html>

Coletta, V. (n.d.). College Physics.

King, A. (1998, November 13). *Inertial Navigation – Forty Years of Evolution*. Retrieved from http://www.imar-navigation.de/downloads/papers/inertial_navigation_introduction.pdf

MEMS Investor Journal, Inc. (2010). *MEMS BASED ATTITUDE AND HEADING REFERENCE SYSTEMS: OVERVIEW AND CURRENT TRENDS*. Retrieved from

Inter-American University of Puerto Rico
Advance Research and Innovative Experience for students
(ARIES)

<http://www.memsinvestorjournal.com/2010/12/mems-based-attitude-and-heading-reference-systems-overview-and-current-trends.html>

NASA. (n.d.). *Earth's Inconstant Magnetic Field*. Retrieved from www.nasa.gov:
http://science.nasa.gov/science-news/science-at-nasa/2003/29dec_magneticfield/

OPEN-LOOP CONTROL SYSTEM. (n.d.). Retrieved from <http://www.tpub.com>:
http://www.tpub.com/content/neets/14187/css/14187_92.htm

O'Reilly, R., Harney, K., & Khenkin, A. (n.d.). *Sonic Nirvana: MEMS Accelerometers as Acoustic Pickups in Musical Instruments*. Retrieved from
<http://www.sensormag.com/sensors/acceleration-vibration/sonic-nirvana-mems-accelerometers-acoustic-pickups-musical-i-5852>

pololu. (n.d.). *Micro Maestro 6-Channel USB Servo Controller*. Retrieved from
<http://www.pololu.com/catalog/product/1350>

Robotzone, LLC. (1999). *Open loop vs closed loop control systems*. Retrieved from www.servocity.com:
<http://www.servocity.com/html/checkout.html>

Robotzone, LLC. (n.d.). *What is a servo?* Retrieved from www.servocity.com:
http://www.servocity.com/html/what_is_a_servo_.html

Sebastian, M. (n.d.). *Automated calibration of an accelerometers*. Retrieved from http://www.x-io.co.uk/res/doc/automated_calibration_of_an_accelerometers_magnetometers_and_gyroscopes_a_feasibility_study.pdf

Senodia. (n.d.). *Working principle of MEMS gyro (Coriolis force)*. Retrieved from
<http://senodia.com/english/products.php>

Strickland, J. (n.d.). *What is a gimbal -- and what does it have to do with NASA?* Retrieved from
[howstuffworks.com](http://www.howstuffworks.com): <http://science.howstuffworks.com/gimbal1.htm>

Watson Industries. (n.d.). *Attitude and Heading Reference System*. Retrieved from http://www.watson-gyro.com/products/attitude_reference_AHRS-S305_spec.html

what-when-how.com. (n.d.). *SPACECRAFT GUIDANCE, NAVIGATION AND CONTROL SYSTEMS*. Retrieved from <http://what-when-how.com/space-science-and-technology/spacecraft-guidance-navigation-and-control-systems/>

Inter-American University of Puerto Rico
Advance Research and Innovative Experience for students
(ARIES)

3.0 Table of Figures

<u>FIGURE 1: HIGH ACCURACY CALIBRATION MECHANISM (HACM)</u>	36
<u>FIGURE 2: CALIBRATION ROUTINE PROGRAM AND GUI USING LABVIEW</u>	37
<u>FIGURE 3: ACCELEROMETER CALIBRATION ON Z AXIS.</u>	38
<u>FIGURE 4: ACCELEROMETER CALIBRATION FLOWCHART</u>	39
<u>FIGURE 5: GYROSCOPE FULL ROTATIONAL MOVEMENT FOR Z AXIS</u>	40
<u>FIGURE 6: GYROSCOPE CALIBRATION FLOWCHART</u>	41
<u>FIGURE 7: CALIBRATION MECHANISM WITH THE APPLIED MAGNET</u>	42
<u>FIGURE 8: MAGNETOMETER CALIBRATION FLOWCHART</u>	43
<u>FIGURE 9: EQUATIONS TO DETERMINE COEFFICIENTS A AND B</u>	44
<u>FIGURE 10: GYROSCOPE X AXIS CALIBRATED DATA VS RAW DATA</u>	49
<u>FIGURE 11: GYROSCOPE Y AXIS CALIBRATED DATA VS RAW DATA</u>	17
<u>FIGURE 12: GYROSCOPE Z AXIS CALIBRATED DATA VS RAW DATA</u>	50
<u>FIGURE 16: ACCELEROMETER X AXIS CALIBRATED DATA VS RAW DATA</u>	49
<u>FIGURE 17: ACCELEROMETER Y AXIS CALIBRATED DATA VS RAW DATA</u>	50
<u>FIGURE 15: ACCELEROMETER Z AXIS CALIBRATED DATA VS RAW DATA</u>	48
<u>FIGURE 16: MAGNETOMETER Z AXIS CALIBRATED DATA VS RAW DATA</u>	49
<u>FIGURE 17: MAGNETOMETER X AXIS CALIBRATED DATA VS RAW DATA</u>	50
<u>FIGURE 18: MAGNETOMETER Y AXIS CALIBRATED DATA VS RAW DATA</u>	50

Inter-American University of Puerto Rico
Advance Research and Innovative Experience for students
(ARIES)

4.0 Calibration Procedure

Calibration is the technique that involves the comparison of two or more measurements, which are analyzed and adjusted to determine estimated misalignment, bias, scale and obtain the values as close as possible to a known measurement of the device this guarantee a high accurate system. On IMU and AHRS devices the calibration procedure is very important, to be able to remove the systematic sensors errors. These errors can generate a notable gap between real and measured data reducing the system performance and accuracy. (Sebastian)

The Calibration of the sensors currently used on the HASP 2010 and 2011 payload was successfully performed for the following sensors accelerometer (SCA-3000) ,Gyroscope (ITG-3200) and Magnetometer(MicroMag3) . The calibration of the sensors was performed using the High Accuracy Calibration Mechanism (HACM) as illustrated in figure 1 , this calibration mechanism utilize three servo motors that can rotate the system with a closed-loop positional position feedback about $\pm 180^\circ$, $\pm 900^\circ$, and $\pm 900^\circ$ independently around the system pitch, roll and yaw axis respectively. The HACM is controlled using a pololu servo controlled that is interfaced to a computer through Labview. Since Labview provides a communication platform with the servo controller a calibration routine was performed using an algorithm as shown in figure 2.

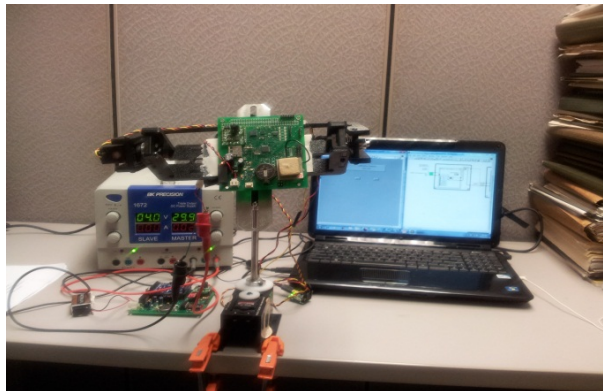


Figure 29: High Accuracy Calibration Mechanism (HACM)

Inter-American University of Puerto Rico
Advance Research and Innovative Experience for students
(ARIES)

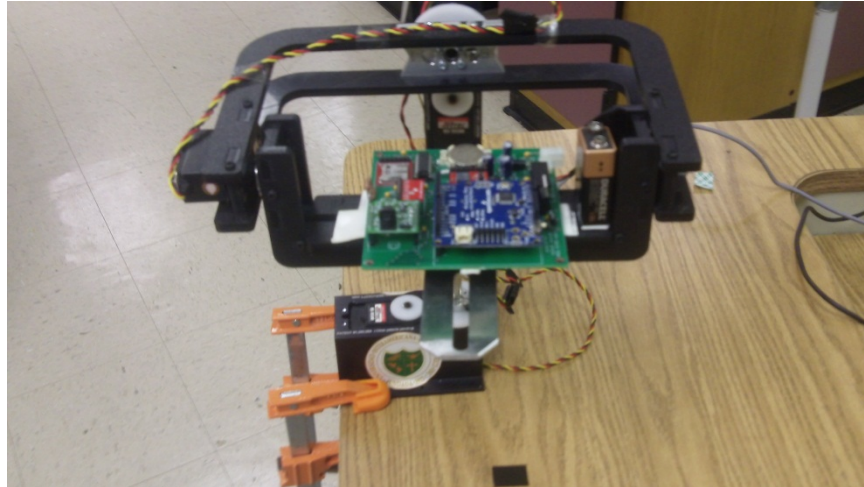


Figure 31: Accelerometer Calibration on Z axis.

Therefore since we have acquired N seconds of data, now we would have a series of acceleration measurements on that selected axis. So let's call this data value $X_{measured1}$, subsequently we applied a linear regression to that data to obtain a single value $x_{measured1}$ for this measurement step:

$$x_{measured1} = \text{Linear Regression} (X_{measured1})$$

Successively we repeat the same process for another known acceleration. This means that in our model, since the chosen axis was pointing up the first time around, we will now rotate the accelerometer so that the chosen axis points on the opposite direction.

Performing this for every axis gather enough information to construct a table:

	real	measured
1 st measurement	X_{real1} (1G)	$x_{measured1}$
2 nd measurement	X_{real2} (-1G)	$-x_{measured2}$

And so we can calculate A and B by simply solving the system:

$$\begin{aligned} X_{real1} &= A x_{measured1} + B \\ x_{real2} &= A x_{measured2} + B \end{aligned}$$

Inter-American University of Puerto Rico
Advance Research and Innovative Experience for students
(ARIES)

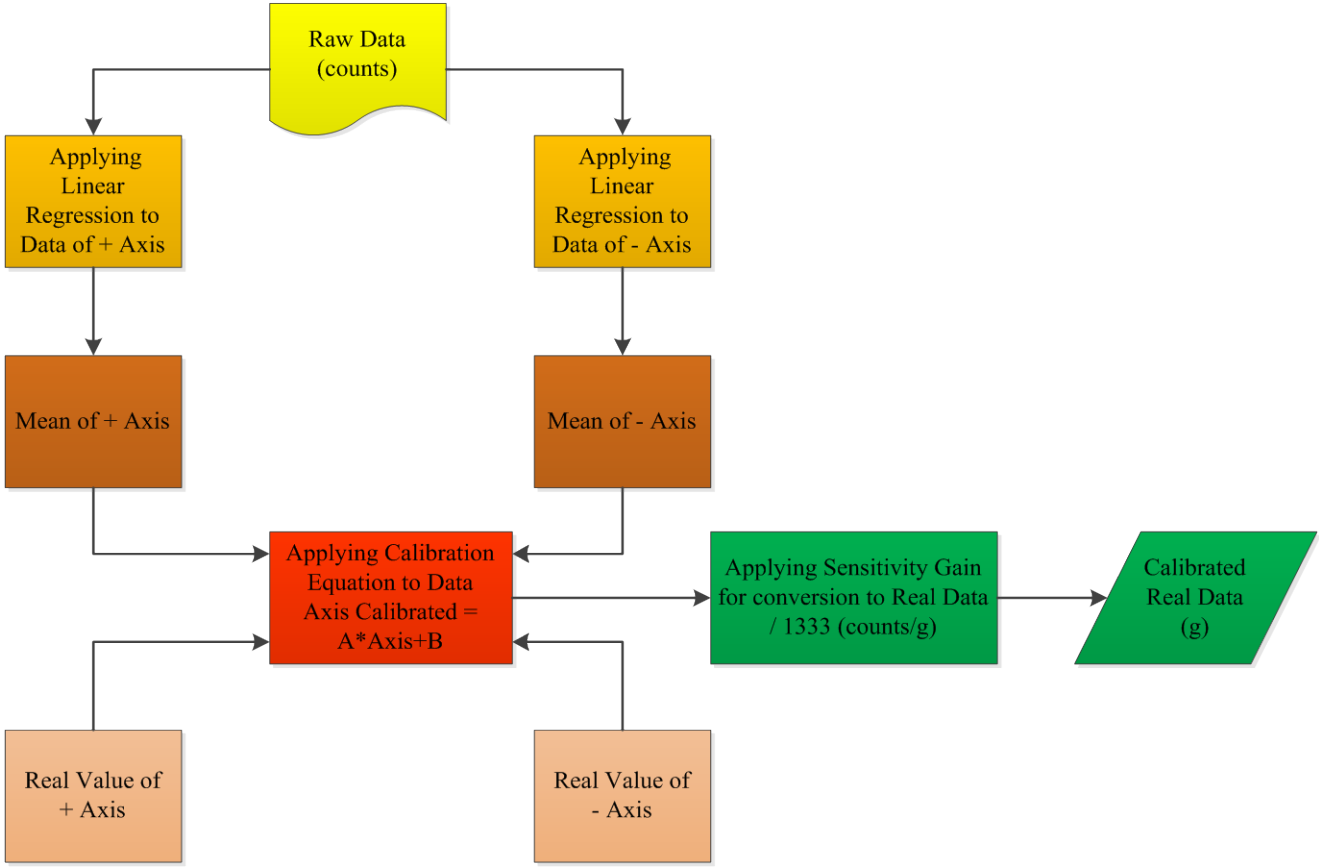


Figure 32: Accelerometer Calibration Flowchart

Inter-American University of Puerto Rico
Advance Research and Innovative Experience for students
(ARIES)

4.1.2 Gyroscope

For the calibration procedure of the gyroscope it's necessary to rotate around one axis by a known angular velocity and ensures that the angular velocity measured by the gyroscope is equal to the known angular velocity. Then be repeated for all three axes (x, y, z). To achieve an accurate calibration, the program collects each gyroscope axis calibration dataset at 1 sample by second during a full rotation around each axis at a constant angular velocity for nearly five minutes. The constant angular velocity is determine by recording the rotation of the HACM using a High Definition camera and performing a video analysis using a professional video editing software.

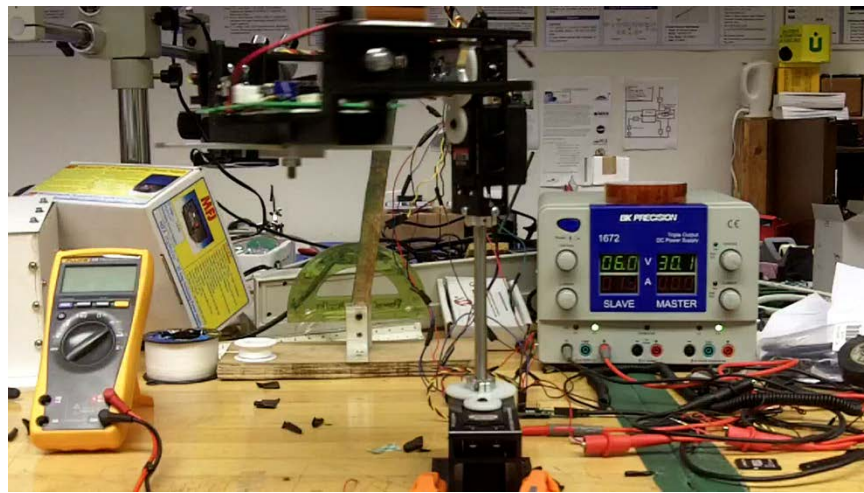


Figure 33: Gyroscope full rotational movement for Z axis

Since we have the constant angular velocities exerted we proceed to repeat the steps used for the accelerometer but for different known rotation speeds instead of different orientations of the sensor. Finally all the data obtained from the sensors throughout the calibration procedure its stored on the SD card to perform the calibration calculations.

Inter-American University of Puerto Rico
Advance Research and Innovative Experience for students
(ARIES)

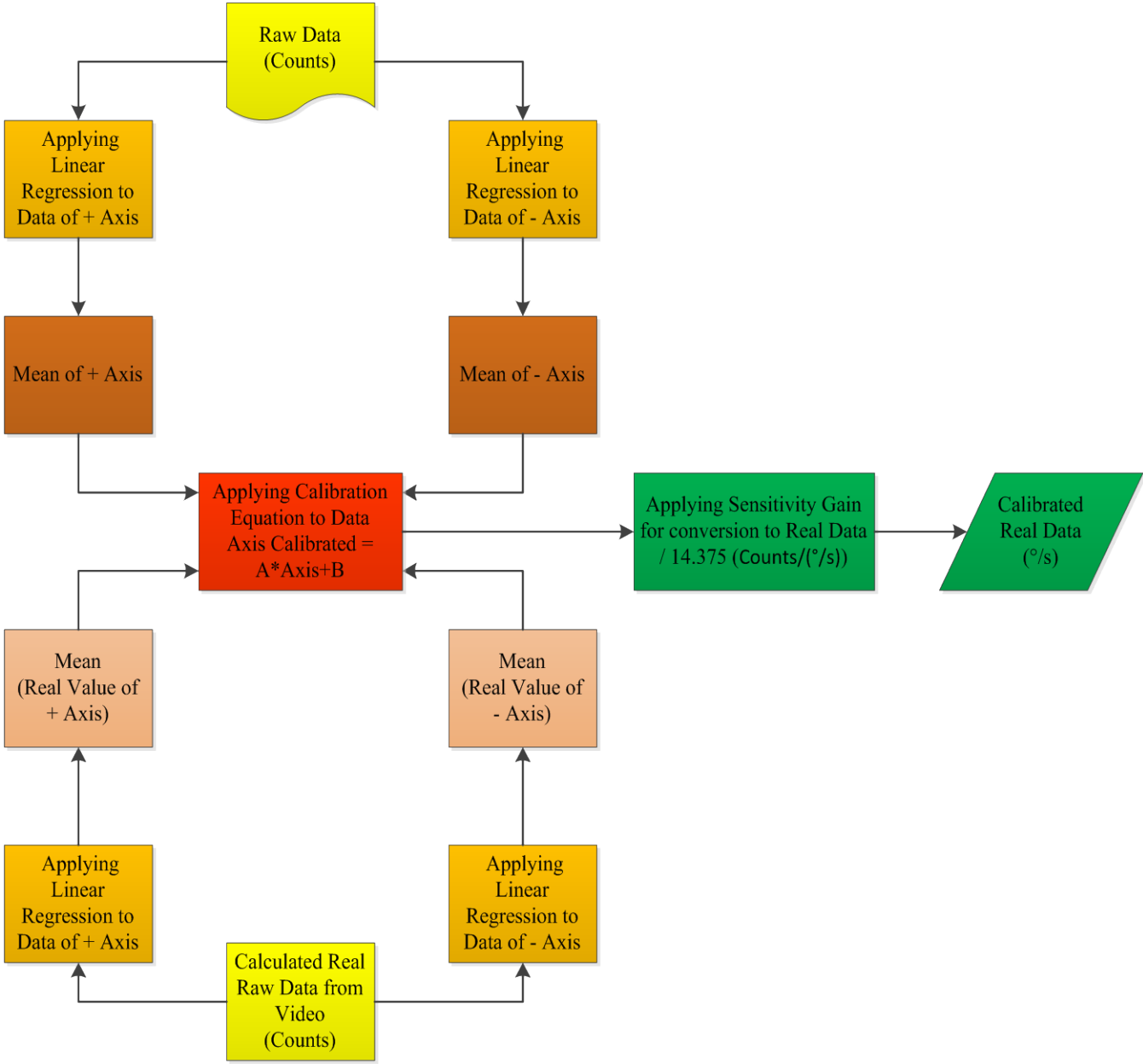


Figure 34: Gyroscope Calibration Flowchart

Inter-American University of Puerto Rico
Advance Research and Innovative Experience for students
(ARIES)

4.1.3 Magnetometer

The magnetometer measurements of the magnetic are usually corrupted by numerous errors including sensor manufacture problems , noise and magnetic deviations induced by electronic equipment, metals and other errors.

To perform the calibration for the magnetometer was necessary to figured out a way to have a known magnetic field value. In that way we can used the same process performed for the accelerometer and gyroscope. This is basically impossible if you don't have access to this type of equipment. For that reason we choose to utilize a speaker magnet to approximately determine the real value of the magnetic field measured by the sensor.

To be able to calculate the magnet field we develop an experiment consisting on gathering data in all three axes (x, y, z) of the magnetometer, then we repeat the process but with the magnet applied. The magnet its applied aligned with z axis and remain at the same position for each orientation as show in figure 7 we only vary the direction of the axis, positive or negative, so we can assumed a constant applied magnetic force in the selected direction.

Then to determine the value of the magnetic field produced by the magnet, we calculate the difference between the raw data with applied magnet and the raw data alone. This operation only produce one value for the axis, positive or negative , since we only have one value its necessary to do the same process for the other component of the same axis.

Therefore performing an average calculation between positive and negative values we can determine approximately the average value of the magnetic field intensity at the selected axis.

Since we have the approximately value of the magnetic field exerted to the axis, now we need to find the real value of the magnetic field on the axis. Therefore its necessary to take the Raw data with the magnet applied and subtract the value of the average magnetic field. Performing this action generates our "Real "value of the calibration equation. Now we can used the same steps employed for the accelerometer to calibrate the magnetometer.

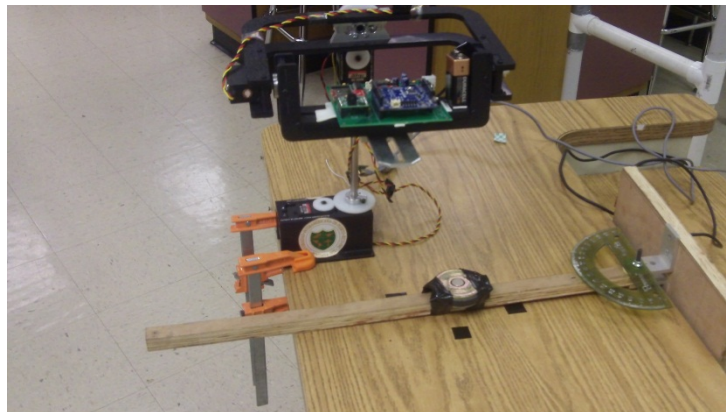


Figure 35: Calibration Mechanism with the applied magnet

Inter-American University of Puerto Rico
 Advance Research and Innovative Experience for students
 (ARIES)

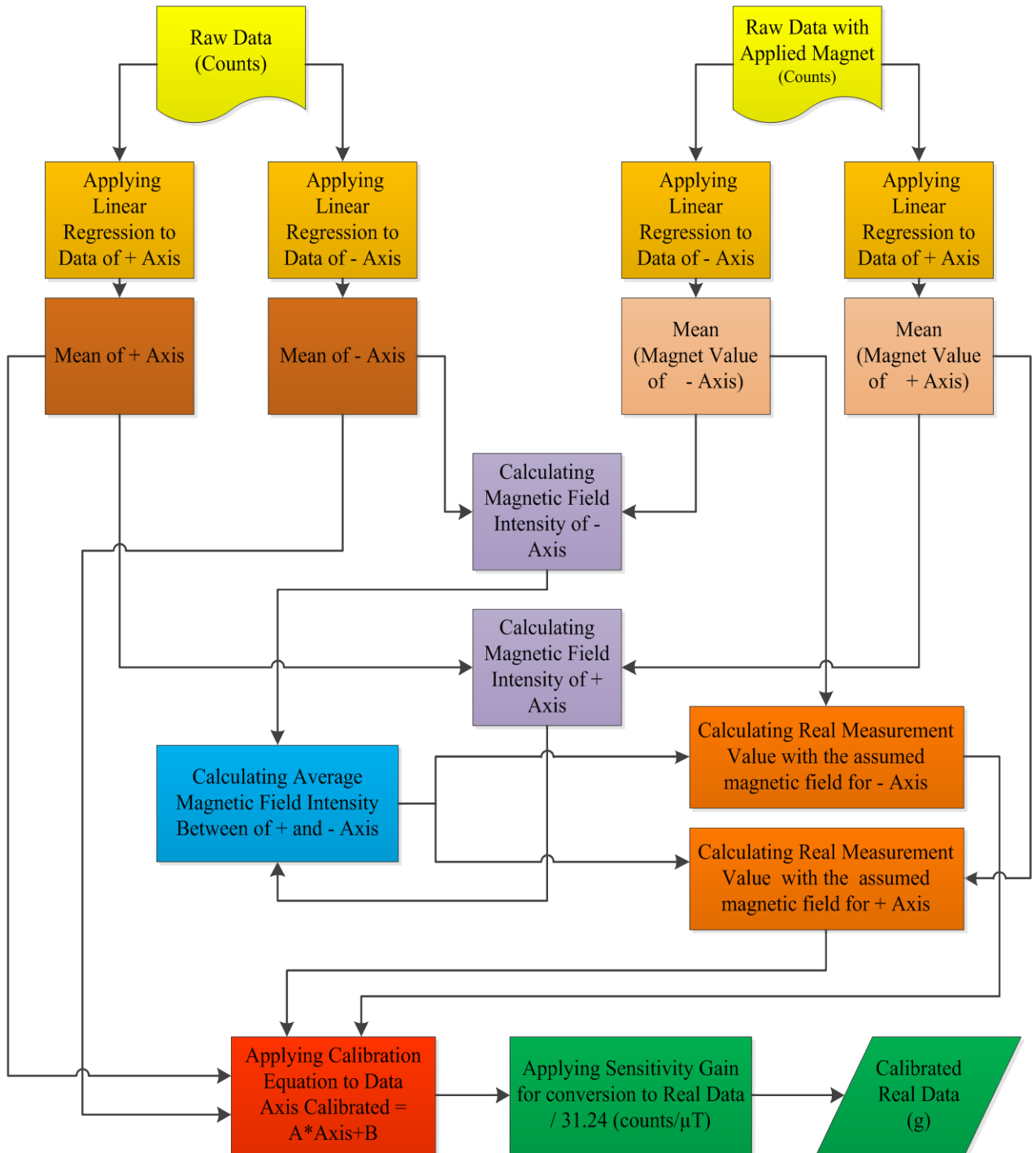


Figure 36: Magnetometer Calibration Flowchart

Inter-American University of Puerto Rico
Advance Research and Innovative Experience for students
(ARIES)

Assuming that the output responses of the sensors are linear with respect to the real value that they are measuring, means that the calibration equation is the same as finding the parameters A and B in the equations below:

$$x_{real1} = A x_{measured1} + B$$

$$x_{real2} = A x_{measured2} + B$$

Where x_{real1} and x_{real2} are the knowing quantities that are used as reference to established the equation.

The $x_{measured1}$ and $x_{measured2}$ are the real value obtained from the sensors and are calculated by performing a linear Regression of the gather data.

The A and B are the two unknowns of the equations. Now by simply solving for A and B we get:

$$B = x_{real1} - A \cdot x_{measured1}$$

$$x_{real2} = A \cdot x_{measured2} + (x_{real1} - A \cdot x_{measured1})$$

$$x_{real2} - x_{real1} = A \cdot (x_{measured2} - x_{measured1})$$

$$A = \frac{x_{real2} - x_{real1}}{x_{measured2} - x_{measured1}}$$

$$B = x_{real1} - \left(\frac{x_{real2} - x_{real1}}{x_{measured2} - x_{measured1}} \right) \cdot x_{measured1}$$

Figure 37: Equations to determine coefficients A and B

Now with the values of A and B for each component. Then is simply to use the calibration equation to obtain calibrated values from the measurements.

Implementation of this equation was performed during the post flight analyze of the data on Dspic33 and arduino obtaining successfully results.

Inter-American University of Puerto Rico
Advance Research and Innovative Experience for students
(ARIES)

4.4 Calibration Results:

This section describes the results obtained through the calibration process performed to the HASP sensors. This calibration procedure generates the following equations for each sensor axis.

Gyroscope

Calibrations results for Gyroscope using the following calculated equations for each axis:

$$X_{axis\ calibrated} = 1.0443 * X_{axis\ measured} + 2.44732$$

$$Y_{axis\ calibrated} = .9744 * Y_{axis\ measured} - .5610$$

$$Z_{axis\ calibrated} = .9962 * Z_{axis\ measured} - .588447$$

Applying this equation directly to the code on the arduino or dsPIC33 microcontroller would display the calibrated data in real time, but to accomplish the analysis these equation were applied to the data stored in the sdcard that contain the HASP flight .Applying these calculation generates the following result:

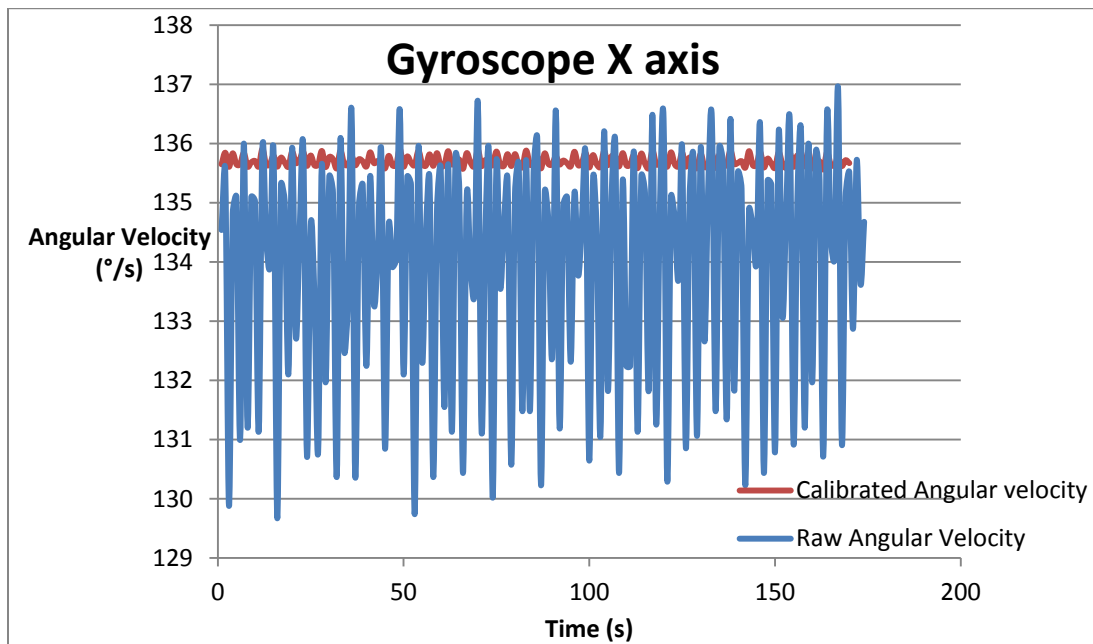


Figure 10: Gyroscope X axis Calibrated data vs Raw data

Inter-American University of Puerto Rico
Advance Research and Innovative Experience for students
(ARIES)

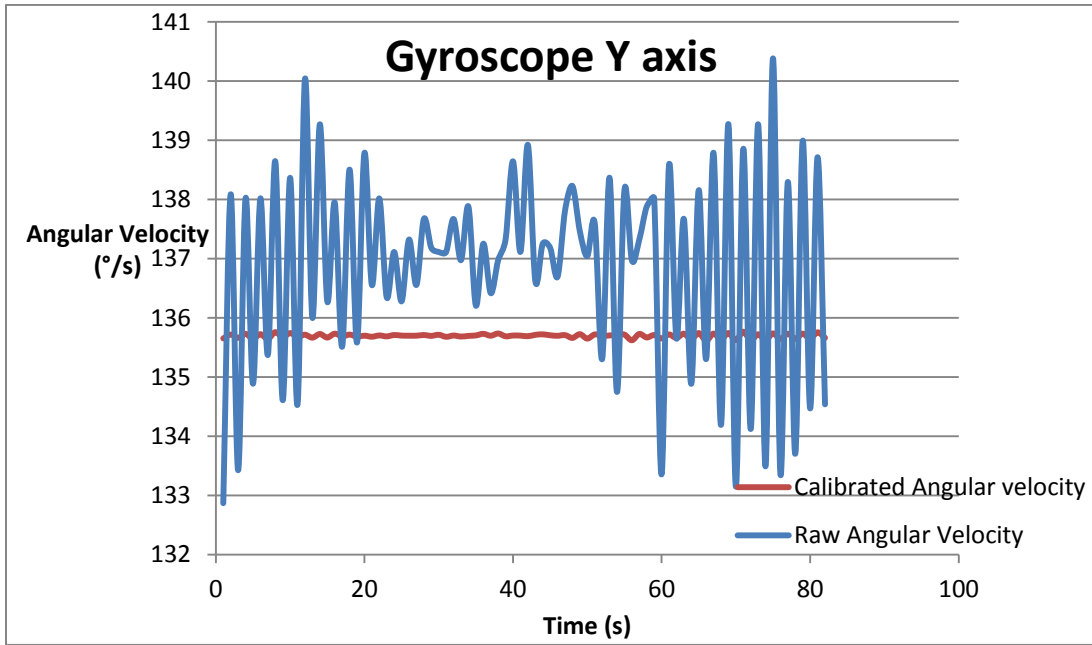


Figure 11: Gyroscope Y axis Calibrated data vs Raw data

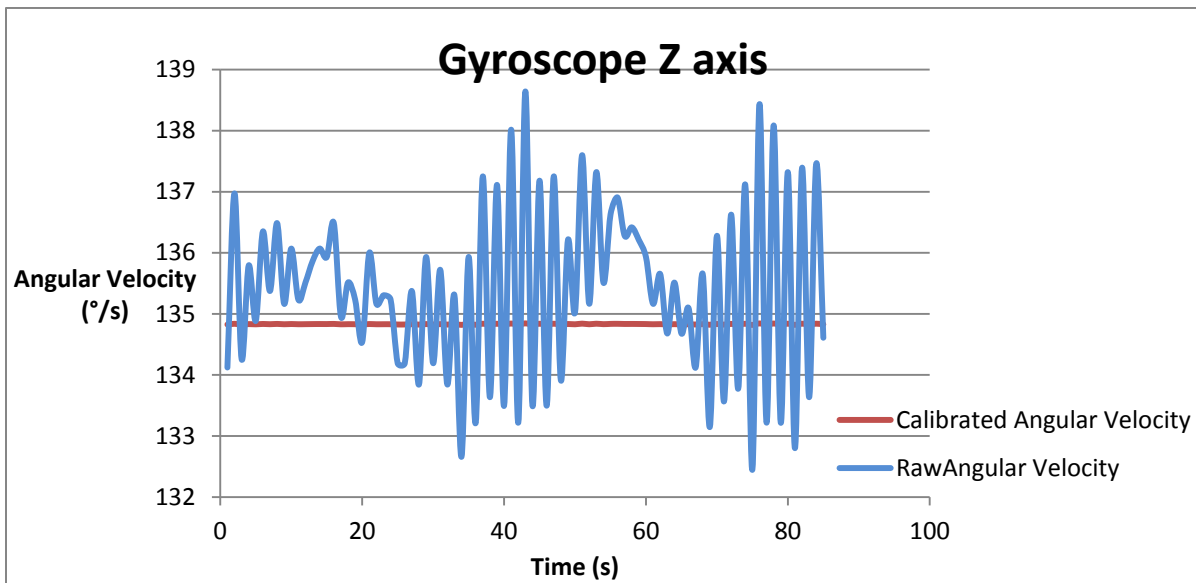


Figure 12: Gyroscope Z axis Calibrated data vs Raw data

The data of the angular velocity obtained during the calibration process for the gyroscope three axes as shown in **Figure 10,11,12** demonstrated the difference between raw data (red) and the calibrated (blue). The first data obtained (raw) contain a lot of noise, high fluctuations and errors in the values that need to be corrected, filtered and calibrated to obtain an accurate real value. Throughout the execution of this calibration we can obtain a new data (calibrated) that is much more precise in comparison with the raw data as illustrated in **Figure 10, 11,12**.

Inter-American University of Puerto Rico
Advance Research and Innovative Experience for students
(ARIES)

Accelerometer

Calibrations results for accelerometer using the following calculated equations:

$$X_{axis\ calibrated} = 1.0032 * X_{axis\ measured} + .02066$$

$$Y_{axis\ calibrated} = 1.0278 * Y_{axis\ measured} - .0659$$

$$Z_{axis\ calibrated} = 1.0119 * Z_{axis\ measured} - .0243$$

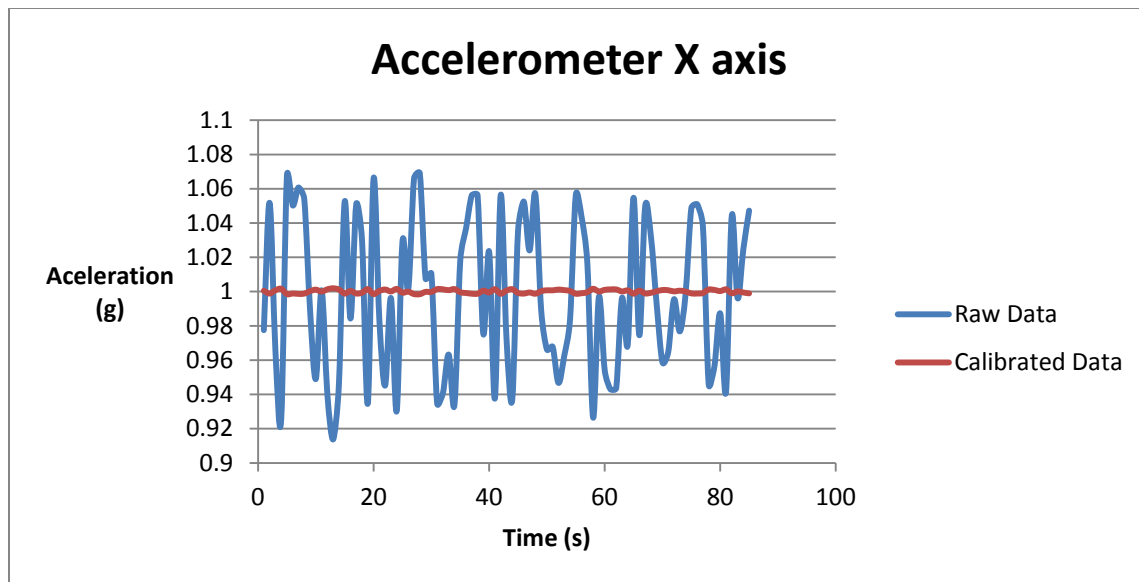


Figure 13: Accelerometer X axis Calibrated data vs Raw data

Inter-American University of Puerto Rico
Advance Research and Innovative Experience for students
(ARIES)

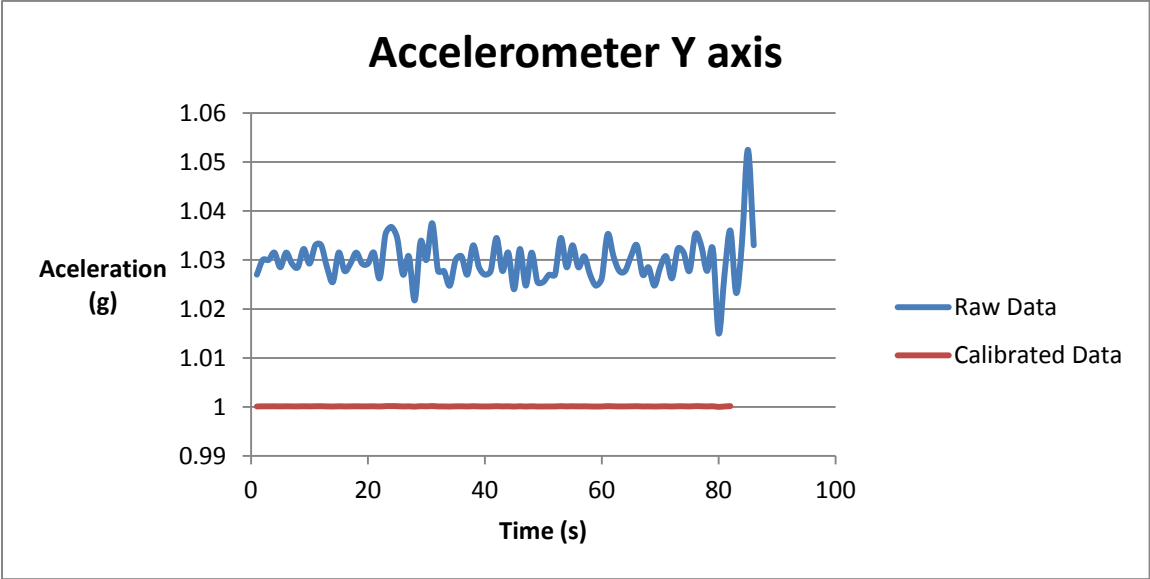


Figure 14: Accelerometer Y axis Calibrated data vs Raw data

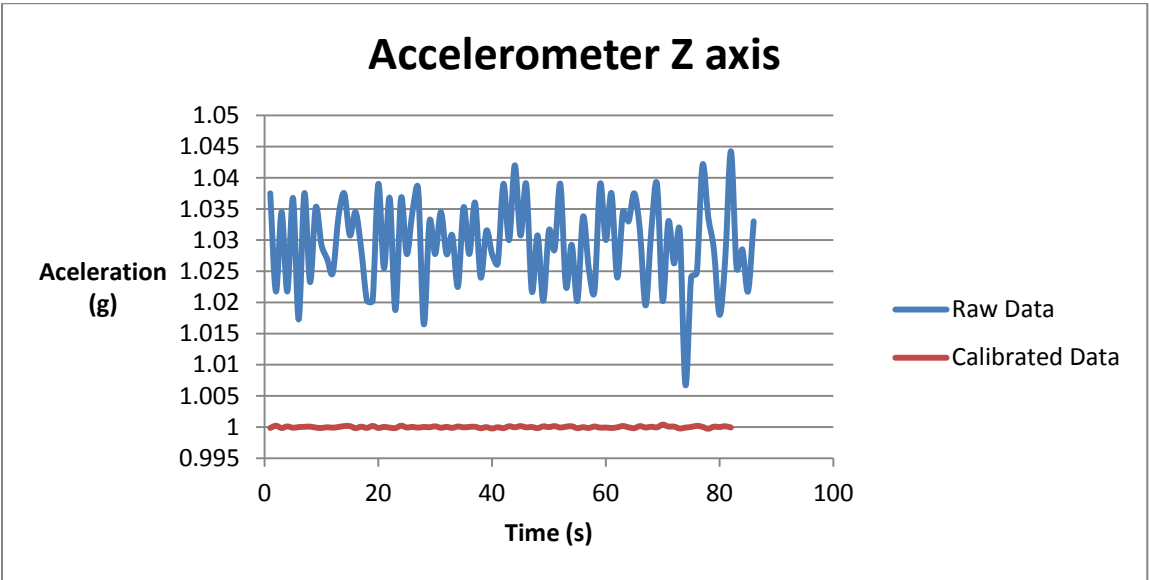


Figure 38: Accelerometer Z axis Calibrated data vs Raw data

The three axes accelerometer data illustrated in **Figure 13, 14, 15** demonstrate the behavior during the flight on the HASP. The data gathered from the accelerometer shows very low fluctuations but some noise in the measure represented with the blue line. Throughout the calibration process of the accelerometer data we manage to attenuate the noise and reduce the fluctuations of the values.

Inter-American University of Puerto Rico
Advance Research and Innovative Experience for students
(ARIES)

Magnetometer

Calibrations results for Magnetometer using the following calculated equations:

$$X_{axis\ calibrated} = (.9999 * X_{axis\ measured\ raw} + 28.97)/31.45$$

$$Y_{axis\ calibrated} = (1.0000 * Y_{axis\ measured\ raw} - 313.9050)/31.45$$

$$Z_{axis\ calibrated} = (1.0000 * Z_{axis\ measured\ raw} - 98.00)/31.45$$

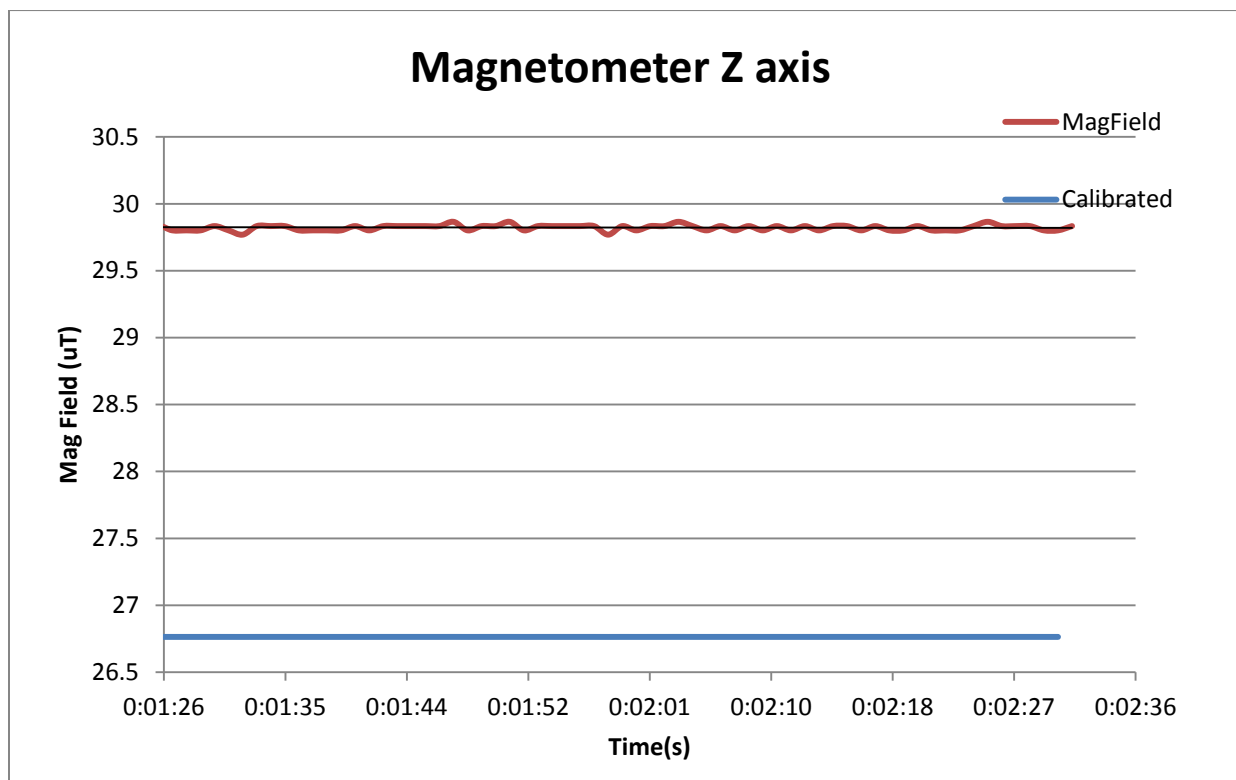


Figure 39: Magnetometer Z axis Calibrated data vs Raw data

Inter-American University of Puerto Rico
Advance Research and Innovative Experience for students
(ARIES)

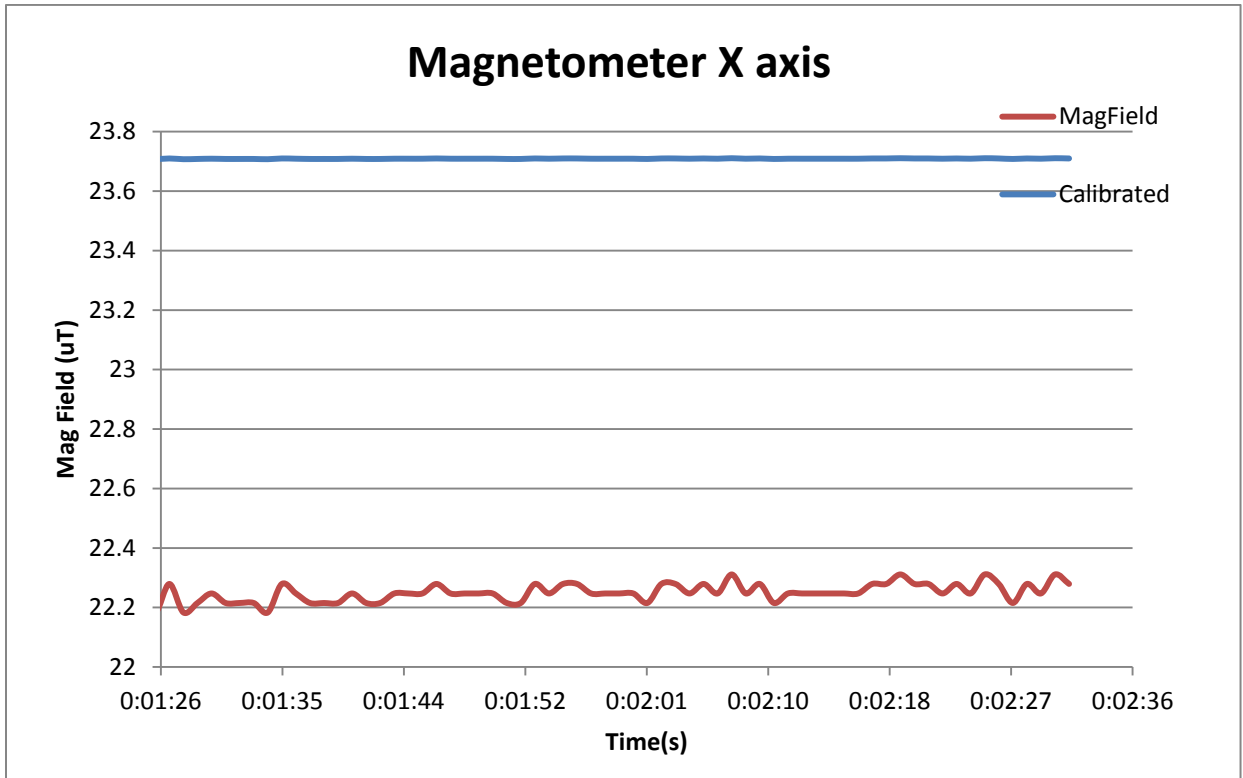


Figure 40: Magnetometer X axis Calibrated data vs Raw data

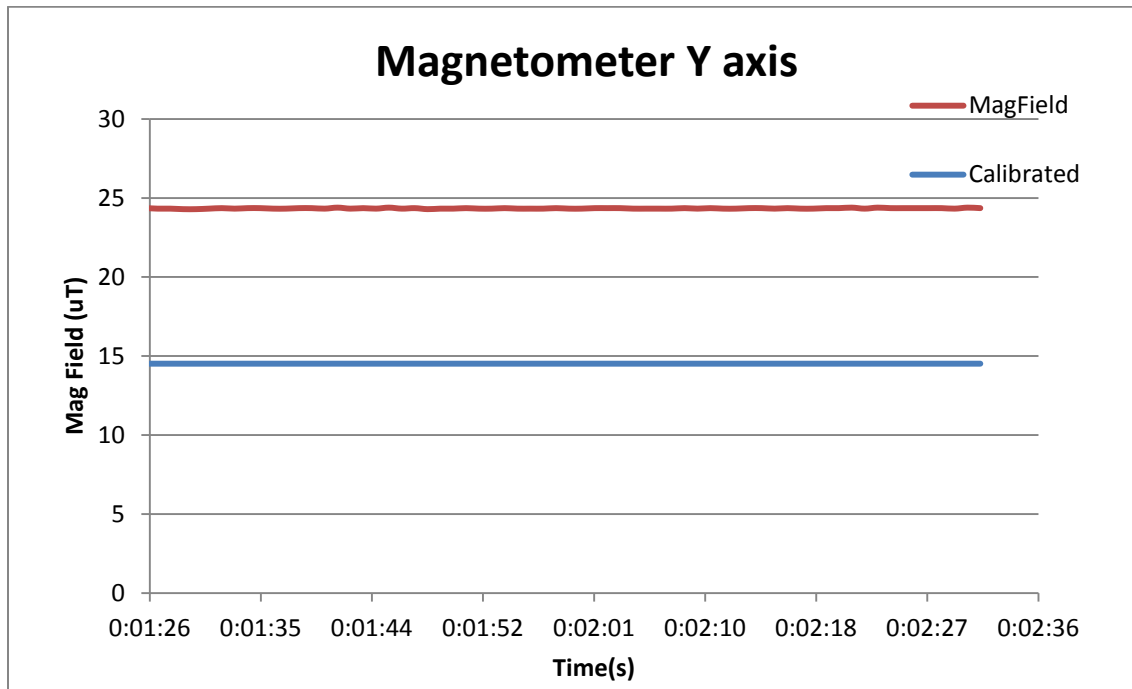


Figure 41: Magnetometer Y axis Calibrated data vs Raw data

Inter-American University of Puerto Rico
Advance Research and Innovative Experience for students
(ARIES)

The data gathered from the magnetometer present the most inaccuracy between raw data and calibrated . This due to the nonexistence of necessary equipment to perform the magnetometer calibration in the best possible way. To be able to obtain an accurate data it is necessary a Helmholtz coil that can generate the know magnetic fields necessary to perform a more accurate calibration. Never less the calibration performed using the available equipment produced the results show in **Figure 16, 17, 18** . These results demonstrate the performance of the calibration, that manage to reduce the noise of the measures but were unable to decrease the fluctuation between values due the calibration equations obtained with the data used. However to achieve a better performance in the future we need to update the equations and apply again to raw data.

5.0 Acknowledgments

This project was accomplished thanks to the help of the following people:

- Dr. Hien Vo, Principal Investigator, UIPR- Bayamón
- Dr. Pedro Capo Lugo, NASA Engineer, NASA Marshall Space Flight Center
- Jose Molina, Graduated Computer Engineering Student, UIPR-Bayamón
- Abel Torres, Undergraduate Computer Engineering Student
- Edwin Pagán, Undergraduate Electrical Engineering Student , UIPR-Bayamón
- Janice Longoria, Undergraduate Mechanical Engineering Student , UIPR-Bayamón
- Ana Espinal , Graduate Electrical Engineering Student , UIPR-Bayamón
- VECTOR Team, Undergraduate Engineering Students , UIPR-Bayamón

Inter-American University of Puerto Rico
Advance Research and Innovative Experience for students
(ARIES)

6.0 Glossary

LAACES	Physics & Aerospace Catalyst Experiences in Research
GUI	Graphical User Interface
AHRS	Attitude Heading Reference System
MEMS	Micro Electrical Mechanical System
TBD	To be determined
TBS	To be supplied
IMU	Inertial Measurement Unit
INS	Inertial Navigation System
SINS	Strapdown Inertial Navigation System
Gyro	Gyroscope
PWM	Pulse Width Modulation